Retrograde mitochondrial signaling governs the identity and maturity of metabolic tissues

Gemma L. Pearson[1*]; Emily M. Walker[1*]; Nathan Lawlor[2,3]; Anne Lietzke[1]; Vaibhav Sidarala[1]; Jie Zhu[1]; Tracy Stromer[1]; Emma C. Reck[1]; Jin Li[1]; Aaron Renberg[1]; Kawthar Mohamed[1]; Vishal S. Parekh[4]; Irina X. Zhang[4]; Benjamin Thompson[4]; Deqiang Zhang[5]; Sarah A. Ware[6]; Leena Haataja[1]; Stephen C.J. Parker[7]; Peter Arvan[1]; Lei Yin[5]; Brett A. Kaufman[6]; Leslie S. Satin[4]; Lori Sussel[8]; Michael L. Stitzel[2,3]; and Scott A. Soleimanpour[1,5,9]

[1]Division of Metabolism, Endocrinology & Diabetes and Department of Internal Medicine, University of Michigan, Ann Arbor, MI, USA.

[2]The Jackson Laboratory for Genomic Medicine, Farmington, CT, USA.

[3]Department of Genetics and Genome Sciences, UConn Health, Farmington, CT, USA

[4]Department of Pharmacology, University of Michigan, Ann Arbor, MI, USA

[5]Department of Molecular and Integrative Physiology, University of Michigan, Ann Arbor, MI, USA

[6]Vascular Medicine Institute, Division of Cardiology, Department of Medicine, University of Pittsburgh School of Medicine, Pittsburgh, PA, USA

[7]Department of Computational Medicine and Bioinformatics, University of Michigan, Ann Arbor, MI, USA

[8]Barbara Davis Center for Diabetes, Department of Pediatrics, University of Colorado Anschutz Medical Campus, Aurora, CO, USA

[9]VA Ann Arbor Healthcare System, Ann Arbor, MI, USA.

*These authors contributed equally to this work

Corresponding Author

Scott A. Soleimanpour, MD, 1000 Wall Street, Brehm Tower Room 6329, Ann Arbor, MI 48105, USA. Phone: (734) 763-0528 E-mail: ssol@med.umich.edu

ABSTRACT

Mitochondrial dysfunction is a hallmark of metabolic diseases, including diabetes, yet the consequences of mitochondrial damage in metabolic tissues are often unclear. Here, we report that mitochondrial dysfunction engages a retrograde (mitonuclear) signaling program that impairs cellular identity and maturity across many metabolic tissues. Surprisingly, we demonstrate that impairments in the mitochondrial quality control machinery, which we observe in pancreatic β cells of humans with diabetes, cause reductions of β cell mass due to dedifferentiation, rather than apoptosis. Utilizing transcriptomic profiling, lineage tracing, and assessments of chromatin accessibility, we find that targeted defects anywhere in the mitochondrial quality control pathway (*e.g.*, genome integrity, dynamics, or turnover) activate the mitochondrial integrated stress response and promote cellular immaturity in β cells, hepatocytes, and brown adipocytes. Intriguingly, pharmacologic blockade of mitochondrial retrograde signaling *in vivo* restores β cell mass and identity to ameliorate hyperglycemia following mitochondrial damage. Thus, we observe that a shared mitochondrial retrograde response controls cellular identity across metabolic tissues and may be a promising target to treat or prevent metabolic diseases.

INTRODUCTION

Mitochondria are vital to cellular bioenergetics in eukaryotes, and mitochondrial defects in numerous tissues are associated with the development of metabolic diseases, such as type 2 diabetes (T2D)[1]. Insulin-producing pancreatic β cells from islet donors with T2D have dysmorphic mitochondrial ultrastructure as well as reductions in the ratio of ATP/ADP following glucose stimulation[2,3]. Skeletal muscle from individuals with T2D exhibits impaired mitochondrial ATP production in response to insulin, reduced mitochondrial respiratory capacity, and decreased mitochondrial (mt)DNA content[4-7]. Further, hepatic mitochondrial uncoupling and proton leak in patients with T2D results in decreases in mitochondrial respiration as well as ATP synthesis and turnover[8-11].

Lowell and Shulman first proposed mitochondrial dysfunction as a unifying mechanism in T2D, and features of mitochondrial impairment have since been described in myocardium, vascular endothelium, adipose tissue, and the central and peripheral nervous systems[1,12]. Importantly, the impact of mitochondrial dysfunction in T2D pathogenesis has been further bolstered by recent work determining that β cell mitochondrial defects precede the development of T2D in humans[13]. Moreover, several human genetic studies support links between mitochondria and T2D[14-19].

Loss of terminal cell identity has recently been observed in several tissues in metabolic diseases. Whereas the maintenance of pancreatic β cell mass was previously believed to depend solely on a balance of β cell replication and apoptosis[20], the loss of β cell differentiation or identity is now recognized as a key factor driving β cell failure in T2D[21-23]. Dedifferentiated or immature β cells lack factors important in fully mature adult β cells, may acquire endocrine progenitor markers, and often express other islet cell hormones[21-23]. Impairments in differentiation have also been observed in other metabolic tissues during T2D[24-26]. However, despite the central importance of mitochondrial dysfunction to T2D, whether mitochondrial dysfunction directly promotes dedifferentiation or immaturity in metabolic tissues is unknown.

Here, we find that mitochondrial dysfunction engages a retrograde mitonuclear signaling program that promotes immaturity in metabolic tissues. Utilizing multiple independent mouse genetic models, metabolic reporters, lineage tracing approaches, and deep sequencing techniques, we observe that loss of mitochondrial quality control elicits dedifferentiation in pancreatic β cells, ultimately leading to loss of β cell mass and hyperglycemia. Importantly, in multiple metabolic tissues—mouse β cells, hepatocytes, brown adipocytes, as well as in primary human islets—mitochondrial dysfunction results in a shared signature including loss of terminal maturity markers, induction of progenitor markers, and activation of the mitochondrial integrated stress response (ISR). Inhibition of the ISR *in vivo* restores β cell mass and maturity and ameliorates glucose intolerance following mitochondrial dysfunction, illustrating that induction of retrograde mitonuclear communication directly promotes dedifferentiation of key metabolic tissues that may be essential to the development of metabolic diseases.

RESULTS

Mitochondrial quality control is impaired in β-cells in T2D

Abnormalities in mitochondrial structure and function have been described in several metabolic tissues in T2D, including pancreatic β-cells[2,3]. Defects in mitochondrial structure and function suggest that mitochondrial defects during the development of T2D may arise due to impairments in mitochondrial quality control or the mitochondrial life cycle, which tightly regulate mitochondrial genome integrity, biogenesis, dynamics, and turnover by mitophagy[27,28]. To investigate these mechanisms, we analyzed human islets from donors with T2D. Human islets from T2D donors exhibited significant reductions in mtDNA content compared to non-diabetic donors (Figure 1A). Concordantly, single cell RNA sequencing (RNAseq) of the β-cells from human islets revealed significantly reduced expression of 11 of the 13 mitochondrially-encoded RNAs (mtRNAs) in donors with T2D (Figure 1B). However, there were no differences in mtRNA levels in α-cells or other non β islet cells between non-diabetic and T2D samples (Figure S1A and [29]), indicating a β-cell specific defect in mitochondrial genome integrity. We also did not observe differences in mitochondrial mass between β cells from non-diabetic and T2D donors, as measured by western blot analysis for OXPHOS subunit proteins and TOM20, suggesting that the reduction in mtDNA content was not secondary to reduced mitochondrial mass (Figure S1B).

As published ultrastructural studies have previously indicated defects in mitochondrial architecture in T2D suggestive of alterations in mitochondrial dynamics[2,3], we next evaluated mitophagic flux in single cells by flow cytometry analysis as per our previous approaches[30-32]. In β-cells from non-diabetic donors, the potassium ionophore valinomycin induced the expected increase in mitophagic flux, defined by cells with increases in depolarized mitochondria within the acidic lysosome compartment (Figure 1C). T2D β cells exhibited lower mitophagic flux following valinomycin exposure, consistent with impairments in mitophagy (Figure 1C). Notably, defects in mitophagy were not observed in non-β cells from T2D donors (Figure S1C), again corroborative of β-cell specific mitochondrial defects in T2D. Taken together, these results indicate that β cells

in T2D exhibit specific defects in mtDNA content, mtRNA levels, mitochondrial structure, and mitophagy, consistent with comprehensive impairments in mitochondrial quality control.

To determine whether changes in β-cell mitochondrial quality control in T2D are secondary to obesity, we measured mtDNA content and mitophagy in transgenic mice expressing the mt-Keima pH sensitive mitophagy reporter[33,34] fed a regular fat diet (RFD) or high fat diet (HFD) for up to one year of age. There were no significant differences in islet mtDNA content secondary to age or diet (Figure S1D). However, we did observe a small, yet significant reduction in the rates of mitophagy in β-cells following diet-induced obesity (DIO) that were not observed in non-β-cells, as measured by flow cytometry (Figure S1E-F). The small reduction in mitophagy without changes in mtDNA content suggests the peripheral effects of obesity or insulin resistance alone do not account for changes in β-cell mitochondrial quality control observed in T2D, and instead suggest an intrinsic defect in β-cells that may be relevant for T2D development and progression.

Mitochondrial quality control is necessary to maintain β-cell mass and function

To determine whether impaired mitochondrial quality control is sufficient to lead to β-cell failure similar to that observed in T2D, we generated several mouse genetic models deficient in components of the mitochondrial quality control machinery. We first generated mice bearing β-cell-specific deletion of Clec16a (*Clec16a*$^{f/f}$; *Ins1*-Cre, hereafter known as β-Clec16a^{KO}; Figure 1D), a critical regulator of mitophagy that is essential to maintain proper mitochondrial clearance and respiratory function [35]. Notably, expression of *Clec16a* is reduced in islets from donors with T2D, and *Clec16a* is also a direct transcriptional target of the T2D gene *Pdx1*[36-38]. β-Clec16a^{KO} mice as well as controls were fed RFD or HFD for 12 weeks prior to physiologic or morphometric assays, and we did not observe differences in insulin sensitivity between genotypes (data not shown). Of note, *Ins1*-Cre and floxed-only controls were phenotypically indistinguishable from each other, exhibiting no differences in glucose tolerance or body weight, and thus were pooled as controls for subsequent analyses, consistent with previous studies from our group and

others[31,39]. RFD-fed β-Clec16a^{KO} mice developed glucose intolerance as expected, and this phenotype was markedly exacerbated in the setting of DIO (Figure 1E). β-Clec16a^{KO} animals also had reductions in serum insulin concentrations upon HFD feeding as well as lower insulin secretion *in vivo* compared to HFD-fed controls (Figures 1F-G).

We next evaluated β-cell mass in mitophagy-deficient mice and observed that β-Clec16a^{KO} animals failed to expand their β-cell mass to compensate for diet-induced insulin resistance (Figure 1H). We did not observe differences in α-cell mass between the groups (Figure S2A). To understand the etiology of reduced β-cell mass in HFD-fed β-Clec16a^{KO} mice, we assessed markers of β-cell proliferation and apoptosis. Surprisingly, we observed a trend toward increased β-cell replication (Figure S2B) with no changes in apoptosis in HFD-fed β-Clec16a^{KO} mice (Figure 1I). Of note, assessments of apoptosis at earlier ages in HFD-fed mice also did not reveal differences between groups (data not shown). Thus, our data led us to speculate that another etiology may contribute to the loss of β-cell mass in this model.

As aging is also a risk factor for the development of T2D[40], we evaluated β-Clec16a^{KO} mice up to one year of age. β-Clec16a^{KO} mice developed severe glucose intolerance and reduced β-cell mass with age, similar to the effect of HFD feeding (Figures S2C-F). To ensure the physiologic and histologic changes we observed were not attributable to developmental defects, we generated inducible β-cell specific Clec16a knockout animals by intercrossing our mice bearing the Clec16a conditional allele with the tamoxifen-inducible MIP-CreERT strain (*Clec16a*$^{f/f}$; *MIP*-CreERT, hereafter known as iβ-Clec16a^{KO} mice). Following tamoxifen-mediated recombination at 7 weeks of age, iβ-Clec16a^{KO} mice exhibited mild glucose intolerance on RFD that was exacerbated upon HFD feeding, reductions in β-cell mass on a HFD, and no differences in β-cell replication or survival when compared to *MIP*-CreERT controls (Figures S2G-J), phenocopying constitutive β-cell Clec16a knockouts. Taken together, these data indicate that mitophagy is vital for the preservation of β-cell mass following aging or obesity, independent of changes in cell replication or survival or defects in β-cell development.

Next, we generated mice bearing reductions of mtDNA content following loss of Tfam, a master regulator of mtDNA copy number control and mitochondrial function, by intercrossing *Ins1*-Cre and *Tfam*$^{f/f}$ mice (hereafter noted as β-Tfam^{KO}; Figure 1J). We chose the *Ins1-Cre* knockin strain to alleviate concerns related to off-target and non-specific effects of the transgenic *RIP2*-Cre strain previously employed to knockout *Tfam*[41,42]. We first observed the expected reductions of mtDNA in β-Tfam^{KO} islets (Figure S2K). To confirm that mtDNA depletion was specific to β-cells, we additionally intercrossed β-Tfam^{KO} mice with the ROSA26-lox-STOP-lox-tdTomato reporter strain, such that β-cells were irreversibly labeled with the tdTomato reporter following Cre-mediated recombination[43]. Following fluorescence-activated cell sorting of tdTomato-positive β-cells, we observed near complete depletion of mtDNA content in β-Tfam^{KO} mice, while tdTomato-negative cells were unaffected (Figure 1K). Similar to Clec16a-deficient mice, β-Tfam^{KO} mice showed progressive glucose intolerance with age, decreased insulin secretion following glucose administration, and markedly reduced β-cell mass without changes in α-cell mass (Figures 1L-N, S2L-N). Interestingly, β-Tfam^{KO} mice also exhibited a significant increase in β-cell replication with only a small increase in apoptosis (Figures 1O-P), which might otherwise be expected to result in a net increase or at least no change in β-cell mass. Analogous to our findings in Clec16a-deficient mice, these results suggest that loss of Tfam markedly reduces β-cell mass and that this effect is unlikely mediated only by control of β-cell replication or survival. Further, these models indicate that defects in mitochondrial quality control lead to progressive loss of β-cell mass and function similar to what is observed in T2D.

Defects in mitochondrial quality control induce loss of β-cell identity

We next asked whether a shared mechanism explained the similarities in phenotypic responses to the orthogonal approaches we used to impair mitochondrial quality control. First, we performed RNAseq on isolated islets from RFD- and HFD-fed β-*Clec16a*^{KO} mice as well as β-Tfam^{KO} mice and their respective controls. Overlaying our results with a previously validated β-cell

maturity/immaturity gene set[44], this approach revealed significant upregulation of genes associated with β-cell immaturity and corresponding downregulation of genes associated with mature β-cells in both RFD and HFD-fed β-Clec16a^{KO} mice as well as islets from β-Tfam^{KO} mice (Figures 2A-B). Gene set enrichment analysis (GSEA) confirmed that genes induced in Clec16a-deficient (Figure 2C) or Tfam-deficient (Figure 2D) mice were significantly enriched for markers of β-cell immaturity. Additionally, pathway analysis identified specific divergences between islets from control and β-Clec16a^{KO} mice. Clec16a-deficient islets displayed downregulation of genes related to insulin secretion and mitochondrial lipid metabolism (β-oxidation and mitochondrial long chain fatty acid oxidation), suggestive of maladaptive β-cell metabolic function. Clec16a-deficient islets also demonstrated increased enrichment for developmental or morphogenetic pathways, including Notch and Id signaling pathways (Figures S3A-B; [45-48]). Similarly, pathway analysis of β-Tfam^{KO} islets displayed downregulation of insulin secretion and key β-cell signature pathways (insulin secretion, maturity onset diabetes of the young, and type II diabetes mellitus) when compared to controls (Figure S4A). Moreover, reduced expression of core β-cell maturity/identity markers, including *Ins2*, *Ucn3*, *Glut2*, and *MafA*, and upregulation of immaturity markers[44,49,50] were commonly observed in both genetic models (Figures 2E-F and S4B-C). Reduced expression of core β-cell maturity markers and increased markers of immaturity were also apparent in islets from mice bearing β-cell-specific deletion of Mitofusins 1 and 2, a recently described model of impaired mitochondrial quality control that abrogates mitochondrial fusion (β-Mfn1/2^{DKO} mice; Figures S4D-E; [31]). Notably, loss of Mfn1/2 also leads to reductions in β-cell mass with age[51]. Stem cell or early endocrine progenitor cell markers such as *Oct4*, *Sox2*, *Nanog*, and *Ngn3* were not upregulated in islets from β-Clec16a^{KO}, β-Tfam^{KO}, or β-Mfn1/2^{DKO} mice (data not shown), indicating that loss of mitochondrial quality control induces markers of immaturity and loss of terminal β-cell identity without a signature associated with regression to early developmental precursors.

To verify changes in β-cell maturity, we performed immunostaining on pancreatic sections from our mouse models. The dedifferentiation marker Aldh1a3, which is not observed in terminally differentiated β-cells but has been found in islets of donors with T2D[21,52], was detectable in RFD-fed β-Clec16a^{KO} mice and further increased upon HFD feeding or aging (Figures 2G and S5A). Aldh1a3 was also upregulated in β-Tfam^{KO}, iβ-Clec16a^{KO}, and β-Mfn1/2^{DKO} β-cells (Figures 2H S5B-C). Further, key β-cell maturation markers Glut2 and Ucn3 were markedly decreased in all these models of impaired mitochondrial quality control (Figures 2I-K, S5D-G).

We next employed genetic lineage tracing to confirm the loss of β-cell identity in Clec16a and Tfam-deficient mice. As noted above, both β-*Clec16a*^{KO} and β-Tfam^{KO} mice (and *Ins1-Cre* control littermates) were intercrossed with the ROSA26-lox-STOP-lox-tdTomato reporter strain[43], such that β-cells were irreversibly labeled with the tdTomato reporter following Cre-mediated recombination. By this lineage tracing strategy, loss of β-cell identity is predicted to result in insulin-negative, tdTomato-positive cells. As expected, >95% of β-cells were positive for both insulin and tdTomato in *Ins1*-Cre control mice, consistent with previous reports (Figure 3A and [39]). No changes in tdTomato lineage allocation were observed between RFD-fed β-*Clec16a*^{KO} mice and controls (Figures 3A-B). However, HFD-fed β-*Clec16a*^{KO} mice had significantly more insulin-negative tdTomato-positive cells compared to HFD-fed controls (Figures 3A-B). We also observed a robust increase in insulin-negative tdTomato-positive cells in Tfam-deficient mice compared to controls (Figures 3C-D). Indeed, the frequency of altered β-cell identity in Tfam-deficient mice was similar to the frequency previously reported following loss of the critical β-cell transcription factor Nkx2.2[53], supportive of a profound impact of mitochondrial quality control on β-cell identity. Surprisingly, we also observed a significant increase in glucagon-positive, tdTomato-positive cells in β-Tfam^{KO} mice, and a similar trend in HFD-fed β-*Clec16a*^{KO} mice, which could indicate that dedifferentiated β-cells acquire glucagon expression (Figures 3E-F). These complementary studies, in multiple independent models resembling mitochondrial dysfunction in T2D, converge to indicate that impaired mitochondrial quality control leads to loss of β-cell identity.

Defective mitochondrial quality control induces the ISR

We hypothesized that impairments in mitochondrial quality control may induce a common mitochondrial-nuclear signaling circuit leading to a transcriptional response consistent with the induction of β-cell dedifferentiation/immaturity. To determine if a common transcriptional signature is activated by mitochondrial dysfunction, we performed a comparative analysis of the top 500 up- and down-regulated genes by RNAseq across our models of mitophagy deficiency (β-Clec16a^{KO}), mtDNA depletion (β-Tfam^{KO}) and defective fusion (β-Mfn1/2^{DKO}). Interestingly, we found 62 upregulated and 29 downregulated genes in common across all three models (Figures 4A-B, Table S1). To search for connections between these targets, we next analyzed these 91 commonly differentially expressed genes by STRING (Search Tool for the Retrieval of Interacting Genes/Proteins; [54]), which revealed two highly connected nodes commonly perturbed by these distinct defects in mitochondrial quality control: (1) an expected change in targets related to mitochondrial-encoded transcripts, and (2) an unexpected interaction relating to key targets in the β-cell maturity and ISR pathways (Figure 4C).

While anterograde signaling from the nucleus to mitochondria has been described in β-cells[36,55], mitochondrial signals that direct nuclear gene expression (*i.e.*, retrograde signaling) have not been observed to date. A candidate pathway to mediate mitochondrial retrograde signaling is the ISR, which coordinates mitochondrial or ER damage responses into a single pathway[56], triggered by phosphorylation of the eukaryotic translation initiation factor Eif2α, which then stabilizes Atf4 to promote downstream transcriptional responses[57]. Indeed, Eif2α phosphorylation and Atf4 protein were significantly increased in β-Clec16a^{KO} islets (Figure 4D). We also observed upregulation of canonical ISR transcriptional targets in RFD-fed β-Clec16a^{KO} mice, which increased to a greater degree upon HFD feeding (Figure 4E). Canonical ISR transcriptional targets were similarly upregulated in β-Tfam^{KO} islets as well as β-Mfn1/2^{DKO} islets (Figures 4F and S5H). Also overexpressed in these models was *Txnip*, which connects

glucotoxicity with mitochondrial damage[58]. Notably, we did not observe signs of ER stress, as we found no increases in expression of the ER chaperone *Bip* in either β-Clec16a^{KO} or β-Tfam^{KO} islets (Figures 4G-H), nor did we observe overt changes in ER morphology in RFD or HFD β-Clec16a^{KO} islets (Figure S6A-D) or β-Mfn1/2^{DKO} islets[31] by transmission electron microscopy (TEM).

To determine if mitochondrial dysfunction elicits the ISR and loss of β-cell maturity in humans, we next generated TFAM-deficient primary human islets using the recently described pseudoislet approach[59]. Briefly, primary human islets were dispersed, transduced with adenoviral particles encoding shRNA targeting TFAM (or scramble controls), and then re-aggregated into pseudoislets. We first confirmed highly efficient TFAM mRNA and protein knockdown 7 days after human pseudoislet formation (Figures 4I-J). We also observed a reduction in expression of mtRNAs following knockdown of TFAM, consistent with impairments in TFAM function (Figure 4I). Consistent with our observation in mouse models, loss of TFAM activated the mitochondrial ISR in human islets, evidenced by Eif2α phosphorylation and ATF4 protein stabilization, induction of ISR transcriptional targets *TRIB3* and *CEBPβ*, increased *TXNIP* expression, and no alterations in *BIP* expression (Figures 4K-L). Further, we observed evidence of loss of β cell maturity following TFAM deficiency in shTFAM-treated human pseudoislets (Figure 4M). Importantly, these results confirm that defects in mitochondrial quality control induce β cell immaturity and the ISR in both mouse and human islets.

Examination of retrograde activating signals implicate energy deficiency in the activation of the mitochondrial ISR

We next assessed the upstream mitochondrial signals that promote the ISR following β-cell mitochondrial dysfunction. The mitochondrial ISR can be activated via reduced energetic output, excess mtROS, or accumulation of misfolded mitochondrial proteins[56]. Indeed, defective metabolic output is among the most potent inducers of the mitochondrial ISR[60-62]. Thus, we first

measured the ATP/ADP ratio with the Perceval biosensor in live β-cells as an indicator of metabolic output following loss of mitochondrial quality control[63]. We observed reduced glucose-stimulated ATP/ADP ratio in islets from β-Clec16a^{KO} mice compared to controls on RFD, which worsened upon HFD-feeding (Figure S7A). These differences occurred without defects in total energetic reserve as measured after exposure to NaN_3 to quench all mitochondrial function (Figure S7A). In islets from β-Tfam^{KO} mice, we observed stark reductions in both glucose-stimulated energetic output and total energetic reserve compared to controls, consistent with a substantial energy deficit (Figure S7B). The more profound effects on both energetic output and β-cell dedifferentiation found in Tfam-deficient compared to Clec16a-deficient islets (Figure 3) are also consistent with the degree of energy deficiency as a driver of the ISR.

We next tested if excess mtROS led to β-cell dysfunction following mitophagy deficiency by intercrossing β-*Clec16a*^{KO} mice (or *Ins1*-Cre controls) with Cre-inducible mitochondrial-targeted catalase (mCAT) overexpressor mice to selectively scavenge β-cell mtROS[64,65]. However, mCAT overexpression, which reduces H_2O_2 as well as superoxide in β-cells[64,65], did not improve glycemic control or insulin secretion in HFD-fed β-*Clec16a*^{KO} mice (Figures S7C-F). Further, we did not observe a consistent increase in markers of the mitochondrial unfolded protein response (UPR^{mt}) across our models of mitochondrial damage (Figure S7G-I), suggesting that mitochondrial protein misfolding and mtROS are unlikely to be responsible for induction of the ISR. Taken together, these results implicate energy deficiency as a primary signal to induce the mitochondrial ISR following defects in β-cell mitochondrial quality control.

Loss of mitochondrial quality control induces chromatin remodeling

To definitively resolve changes in the transcriptional landscape of β cells following loss of mitochondrial quality control, we applied both single-nucleus RNAseq and ATACseq to assess chromatin remodeling that may be altered by mitochondrial retrograde signaling. UMAP plots of snRNAseq and snATACseq data revealed highly distinct populations of β cells of HFD-fed β-

Clec16a^{KO} mice compared to controls (Figures 5A). These results were supported by pathway analyses, which found significant differences between biological processes in β cells from control and β-Clec16a^{KO} mice (Figures S8A-B). Indeed, the snRNAseq results revealed enriched expression of targets associated with insulin secretion in control β cells when compared to Clec16a-deficient β cells (Figures S8A-B). Analysis of snATACseq data revealed 25,016 putative *cis*-regulatory elements uniquely detected as chromatin accessibility peaks unique to Clec16a-deficient β cells, with 3,567 peaks that were absent when compared to control β cells (Figure 5B). These changes included dramatic loss of chromatin accessibility at multiple sites in the *Ins2* locus and accessibility gains in the *Atf3* locus in Clec16a-deficient β cells (Figures 5C-D).

Enrichment analysis of differentially accessible peaks in *Clec16a*-deficient β cells using the Genomic Regions Enrichment of Annotations Tool (GREAT; [66]) revealed the loss of peaks in regions related to the regulation of mitophagy, lysosomal transport, and glucose metabolic processes, consistent with known functions for Clec16a ([35,67]; Figure S8C). In contrast, GREAT peaks uniquely accessible in *Clec16a*-deficient β cells were enriched in regions related to cellular responses to carbohydrate stimulus, abnormal pancreas development, and abnormal pancreatic β cell differentiation (Figure S8D). Importantly, we observed significant enrichment of transcription factor binding site motifs for key ISR transcription factors in Clec16a-deficient β cells by HOMER[68], with bZIP factors, including Atf4, Atf3, and CHOP, the most enriched in β-Clec16a^{KO} mice (Figures 5E-F). Increased binding sites for Bach2, a transcription factor which is associated with β cell immaturity in T2D[69], were also found in Clec16a-deficient β cells (Figures 5E-F). We additionally observed loss of binding sites for transcription factors known to be vital for β cell maturity, identity, and function in Clec16a-deficient β cells, most notably the critical β cell transcription factor and maturity regulator NeuroD1, as well as more broadly expressed transcription factors Sp1 and CTCF (Figures 5E-F; [70-72]). Taken together, these results suggest that mitochondrial retrograde signals lead to substantial modification of chromatin accessibility favoring transcriptional activation of the ISR and loss of cell identity and maturity.

Loss of mitochondrial function induces immaturity and the ISR in hepatocytes and brown adipocytes

Given the critical importance of mitochondrial health in metabolic tissues, we next asked if defects in mitochondrial quality control induce comparable impairments in cell maturity in other metabolic tissues. To this end, we generated mice bearing liver-specific deletion of Mfn1/2 or Tfam, by intraperitoneal administration of adeno-associated virus 8 expressing Cre-recombinase under control of the hepatocyte-specific *Tbg* promoter (AAV8-Tbg^{cre}) to 12-week-old HFD-fed control mice, and *Mfn1/2*- or *Tfam*-floxed animals (hereafter known as L-Mfn1/2^{DKO} or L-Tfam^{KO} mice, respectively; Figures 6A-C). In both models, we observed expected decreases in mtDNA content and alterations of expression of OXPHOS subunits, including reduced Ndufb8 and mt-Co1 and increased Sdhb and Atp5a, without overt reductions in the mitochondrial mass marker Tom20 (Figures 6D-I). L-Mfn1/2^{DKO} animals developed alterations in glucose tolerance and insulin sensitivity consistent with reduced hepatic glucose output, whereas L-Tfam^{KO} mice developed slight alterations in insulin sensitivity with notable hepatic lipid accumulation (Figures S9A-D). Signs of hepatic dysfunction were also evident following loss of mitochondrial quality control, with significant decreases in serum cholesterol in L-Mfn1/2^{DKO} mice and increases in serum ALT and LDH in L-Tfam^{KO} mice (Figures 6J-L). Consistent with our observations in β cells, loss of mitochondrial quality control also did not induce apoptosis in hepatocytes (Figure S9E).

We next used RNAseq to begin to determine if loss of mitochondrial quality control promoted a common signature of activation of the mitochondrial ISR, induction of cell immaturity, and loss of terminal cell identity markers in hepatocytes. As observed in β cells, L-Mfn1/2^{DKO} or L-Tfam^{KO} mice had significantly increased expression of canonical ISR targets without upregulation of *Bip* expression (Figure 6M). To determine if defects in mitochondrial quality control altered hepatocyte maturity, we overlaid the RNAseq data with a curated list of key hepatocyte terminal identity and developmental markers[73]. We found decreased expression of terminal

hepatocyte markers including genes associated with cytochrome P450 activity and bilirubin glucuronidation, and increases in several markers of hepatocyte immaturity, including alpha fetoprotein (*Afp*), *Top2a*, and *Psat1* ([73]; Figures 6N-O). Moreover, western blot analysis confirmed induction of the ISR by detection of increased Atf4 protein levels and Eif2α phosphorylation, reduced levels of mature hepatocyte proteins (Cyp2e1, Mup-3), and increased levels of markers of hepatocyte immaturity (Afp, Top2a, Psat-1) in both L-Mfn1/2^{DKO} and L-Tfam^{KO} mice (Figures 6P-S).

Mitochondrial health is also crucial for brown adipocyte tissue (BAT) function[74], therefore, we next surveyed expression of terminal identity markers and the ISR from mice bearing adipocyte-specific deletion of cardiolipin synthase (Crls1), an enzyme essential for biosynthesis of the key mitochondrial phospholipid cardiolipin[75]. Cardiolipin plays several crucial roles in mitochondrial health, including regulation of mitochondrial quality control through cardiolipin-dependent mitophagy[76,77]. To this end, we analyzed publicly available RNAseq data from BAT depots isolated from mice bearing adipocyte-specific deletion of *Crls1* generated by intercrossing *Crls1* floxed animals with the adiponectin Cre-recombinase strain (hereafter known as AdCKO mice; [75]). AdCKO mice were previously reported to develop impaired mitochondrial function, glucose uptake, and thermogenesis in BAT depots, however, a link between cardiolipin metabolism and BAT maturity was not assessed[75]. To address this question, we evaluated differentially expressed genes between AdCKO and control BAT depots for targets from the BATLAS database, which includes numerous key terminal BAT identity/maturity markers[78]. We found a striking and significant downregulation of 78 of 119 BATLAS genes in AdCKO BAT depots, including a loss of BAT-specific genes associated with cellular maturity/identity, such as *Ppargc1α* and *Ucp1* (Figure 6T). Further, we observed an induction of canonical ISR transcriptional targets in AdCKO BAT depots (Figure 6T). Taken together, these results highlight the vital role for mitochondrial health in promoting terminal cell identity by restraining mitochondrial retrograde signaling in numerous metabolic tissues.

Blockade of retrograde signaling restores β-cell mass and maturity *in vivo*

Our results in numerous metabolic tissues suggest that mitochondrial dysfunction engages the ISR and induces loss of terminal cell maturity/identity. We, therefore, hypothesized that induction of retrograde mitochondrial signaling through the ISR directly leads to loss of cellular maturity. To test the importance of the ISR in β-cell maturity, we treated HFD-fed β-Clec16a^{KO} mice with ISRIB, a well-established pharmacologic inhibitor of the ISR[79]. We first treated isolated islets from HFD-fed β-Clec16a^{KO} mice and controls with ISRIB for 24 hours, observing the expected reduction of ISR transcriptional targets, including *Cebpβ* and *Trib3*, in islets from HFD-fed β-Clec16a^{KO} mice (Figures 7A-B). Concordantly, we found that ISRIB restored expression of the terminal β-cell identity marker *Ucn3* and reduced expression of the dedifferentiation marker Aldh1a3 in islets from HFD-fed β-Clec16a^{KO} mice (Figures 7C-D). To determine if the restoration of β-cell identity was related to an unanticipated upregulation of mitophagy in Clec16a-deficient β-cells, we intercrossed β-Clec16a^{KO} mice with the mt-Keima mitophagy reporter strain to assess mitophagy flux (Figure 7E). Importantly, ISRIB did not ameliorate the well-known defects in mitophagy flux associated with Clec16a-deficiency (Figure 7E), suggesting the restoration of β-cell identity markers by ISRIB was not due to improved mitophagy but rather related to blockade of retrograde signaling through the ISR.

To next determine if retrograde signaling through the ISR leads to loss of β-cell mass and identity *in vivo*, we treated HFD-fed β-Clec16a^{KO} mice and littermate controls with ISRIB by daily intraperitoneal administration for 4 weeks (Figure 7F). Notably, extended treatments with ISRIB in control animals *in vivo* did not impair β-cell mass, glucose tolerance, or insulin sensitivity (Figures 7G-J), consistent with a previous report [80]. Intriguingly, ISR inhibition rescued the loss of β-cell mass in HFD-fed β-Clec16a^{KO} mice (Figure 7G). ISRIB treatment also ameliorated glucose intolerance in HFD-fed β-Clec16a^{KO} mice, while peripheral insulin sensitivity was unchanged between groups (Figure 7H-J). Importantly, ISRIB treatment reduced expression of Aldh1a3 in

HFD-fed β-Clec16a^{KO} mice and increased the frequency of Ucn3-positive β cells bearing proper expression/localization of Glut2, consistent with restoration in β cell maturity and identity (Figures 7K-P). Notably, the benefits of ISRIB on β-cell mass and identity are unlikely to be due to an indirect mitigation of chronic hyperglycemia, as treatment with the SGLT1/2 inhibitor phlorizin to improve glucose homeostasis by increased glycosuria did not rescue β-cell mass or function in mitophagy-deficient mice (Figures S10A-E). Taken altogether, these studies position the induction of mitochondrial retrograde signaling through the ISR as a direct regulator of cell maturity and identity in metabolic tissues.

DISCUSSION

Mitochondria are pivotal cellular organelles, which provide the energy required for cellular function, growth, division, and survival. Here, we demonstrate that mitochondrial dysfunction engages a retrograde signaling response shared across metabolic tissues, which ultimately impairs cellular identity and maturity. Perturbations at any point within the mitochondrial quality control machinery converge to activate the ISR, eliciting a transcriptional signature associated with induction of cellular immaturity and modulation of chromatin architecture. Intriguingly, changes in terminal cell identity are reversible, as inhibition of the mitochondrial ISR restores cellular maturity, mass, and function. Together, our results demonstrate that mitochondrial function plays a central role in the control of cell identity in metabolic tissues.

Our studies implicate a crucial role for retrograde mitochondrial control of cellular identity and maturity. Our results were also surprising as mitochondrial dysfunction has been classically associated with a decline in proliferation or survival. Retrograde signals generated from the mitochondria in yeast to activate the transcriptional regulators Rtg1, 2, and 3 have been well characterized[81-83], yet mammalian orthologs of these factors have proved elusive to date. Indeed, retrograde signaling has unclear roles in the regulation of mammalian cellular homeostasis[56,84,85]. Interestingly, the Rtg family has been implicated in the modulation of TCA cycle enzymes, glutamate biosynthesis and mtDNA maintenance, but not in cellular identity[83]. Although mammalian Rtg orthologs have yet to be discovered, distinct retrograde signaling pathways are present in mammalian cells, including the UPR^{mt} and the ISR. Activation of the UPR^{mt} and the ISR have been previously implicated in the regulation of cell survival, yet the control of cellular identity or maturity have not been described[56]. Thus, our studies position a new role for retrograde signaling following mitochondrial dysfunction to impair cellular maturity, ultimately leading to the deterioration of metabolic tissues.

Our results identifying the crucial importance for mitochondria to direct cellular maturity and identity additionally resolve confusion regarding anterograde (*i.e.*, nuclear to mitochondrial)

control of cell fate across metabolic tissues. Instances of anterograde control of cellular maturity and identity have been reported; however these transcriptional regulators, including Foxo1, Prdm16, Pgc1α, ERRγ, and Pdx1, possess unique tissue-specific effects and have not been demonstrated to directly regulate both cellular maturity and mitochondrial metabolism uniformly across metabolic tissues[36,86-90]. For instance, Foxo1 deficiency promotes β cell dedifferentiation via control of the NADH-dependent oxidoreductase Cyb5r3, which localizes to membranes in the ER, mitochondria, and plasma membrane[22,91,92]. In contrast, Foxo1 deficiency promotes BAT differentiation and has not been shown to lead to dedifferentiation in adult hepatocytes[93-95]. Further, Pgc1α, while crucial for BAT maturity and mitochondrial function, is dispensable for β cell maturity and mitochondrial function[87,96-98]. ERRγ induces postnatal maturation of β cells and BAT while activating expression of numerous mitochondrial genes; however, ERRγ deficiency has not been previously implicated in the development of hepatocyte immaturity via mitochondrial dysfunction[90,99,100]. Due to their tissue-specific effects, many of these transcriptional regulators regulate additional mitochondria-independent processes, rendering it challenging to conclude that regulation of mitochondrial function by these nuclear factors is solely sufficient to maintain cellular maturity and identity across metabolic tissues. Thus, our studies obviate these concerns by establishing the central importance of mitochondrial health to maintain cellular maturity and identity across metabolic tissues.

We observe substantial changes in chromatin accessibility following the induction of mitochondrial dysfunction and activation of the ISR. The increased frequency of binding motifs related to the central ISR transcriptional regulator ATF4, as well as ATF4 targets, is suggestive that retrograde signaling may also alter chromatin structure. Indeed, ATF4 is a pioneer factor capable of altering chromatin accessibility[101], which could be consistent with the transcriptional signatures observed in metabolic tissues with mitochondrial damage. However, it is unclear how the induction of ATF4 remodels sites of chromatin accessibility that are lost at key markers of β

cell maturity, such as NeuroD1[70]. Loss of binding regions essential for β cell maturity following mitochondrial dysfunction could also be secondary to impaired substrate availability and metabolism, eventually affecting epigenetic modifications, similar to metabolic control of epigenetics reported in the cancer biology literature[102]. Thus, we speculate that defects in bioenergetic capacity following mitochondrial dysfunction could have a cascade of effects, initiated by activation of the ISR, to remodel chromatin architecture, and drive dedifferentiation to an immature state. Therefore, exploration of the control of chromatin accessibility following mitochondrial dysfunction, and how retrograde metabolic signals may be tuned by sensors of the ISR, including the kinases PERK, GCN2, HRI, and PKR[103], will be intriguing avenues for future study.

Mitochondrial health is central to the function of metabolic tissues, yet mitochondria are frequently viewed as client organelles rather than as primary drivers of cell fate. Indeed, the appearance of mitochondrial dysfunction in metabolic tissues during diabetes or other metabolic diseases is often considered an indirect consequence of other etiologies, including transcriptional defects, ER stress, or nutritional excess[104-106]. Here, we observed key defects across the spectrum of the mitochondrial quality control pathway in human β-cells during T2D that are each sufficient to elicit β-cell immaturity in isolation in genetic mouse models or primary human islets. The remarkable consistency of these connections between mitochondrial dysfunction and cellular immaturity across human and mouse metabolic tissues further supports the central importance of mitochondria in maintaining terminal cell identity, which to our knowledge has not previously been described. Interestingly, our results suggest the loss of mitochondrial quality control across metabolic tissues lead to distinct effects from other cell types, such as renal epithelial cells, which develop activation of the cytosolic cGAS-stimulator of interferon genes (STING) DNA sensing pathway, cytokine expression, and immune cell recruitment upon Tfam-deficiency[107]. We did not observe evidence for activation of cGAS-STING or cytokine expression across our models of mitochondrial dysfunction, including both β-Tfam^{KO} and L-Tfam^{KO} mice, suggesting the

development of immaturity upon mitochondrial dysfunction may be unique to metabolic tissues and is unlikely to involve a type I interferon response. Studying these cell type-specific responses will be a captivating topic for future investigation.

Our data suggest that blockade of retrograde signaling can prevent the loss of β-cell mass and glycemic control following mitochondrial dysfunction. Our findings reinforce the importance of signatures of mitochondrial dysfunction in human β-cells of pre-diabetic donors with impaired glucose tolerance, potentially indicating that mitochondrial dysfunction preceding T2D may be an etiopathological defect in β-cells that possibly extends to other tissues. While the primary focus of this work was to define a central mechanism underlying mitochondrial control of cell fate in metabolic tissues, future studies will be of keen interest to explore if ISRIB treatment can restore β-cell maturation and glycemic control in T2D as well as in T1D, where blockade of β-cell stress responses are capable of diabetes prevention[108,109]. Moreover, it will be fascinating to determine if preemptively targeting mitochondrial health or retrograde signaling throughout metabolic tissues could prevent the onset of metabolic diseases.

RESOURCE AVAILABILITY

Lead Contact

Further information and request for resources and reagents should be directed to and will be fulfilled by the lead contact, Scott Soleimanpour (ssol@med.umich.edu)

Materials Availability

Rabbit polyclonal Clec16a antisera is available upon request from the lead author. mtKeima mice were maintained on the C57BL/6N background and intercrossed to Clec16a$^{f/f}$ mice to generate mtKeima-Ctrl and mtKeima-β-Clec16a^{KO} mice; these mice are available on request from the lead author.

Data Availability

Bulk RNA-seq, single nuclei RNA-seq and single nuclei ATAC-seq data have been deposited at GEO and are publicly available as of the date of publication. This paper also analyzed existing publicly available data. Microscopy data will be shared by lead contact on request.

Any additional information required to reanalyze the data reported in this paper is available from the lead author on request.

EXPERIMENTAL MODEL AND SUBJECT DETAILS

Genetically modified mouse lines*:* All mice were maintained in accordance with the University of Michigan's Institutional Animal Care and Use Committee under specific pathogen-free conditions. Up to 5 mice were housed per cage and were maintained on regular chow or high fat diet chow with *ad libitum* access to food on a 12 h light-dark cycle. Floxed Tfam (Tfam$^{f/f}$ mice (Jackson Laboratories, Stock no. 026123)), Clec16a (Clec16a$^{f/f}$ mice[35]), Mfn1/2 (Mfn1$^{f/f}$/Mfn2$^{f/f}$ mice (Jackson Laboratories stock no. 026401 and 026525), Rosa26 lox-STOP-lox tdTomato reporter mice (Jackson Laboratories, Stock no. 007914), and floxed stop mCAT overexpression mice (Jackson Laboratories, Stock no. 030712) were used. All animals were maintained on a 100% C57BL/6N background. To generate β-cell specific deletion, floxed models were crossed with Ins1-Cre mice from Jackson laboratories (JAX Stock No. 026801). *Ins1*-Cre–alone and respective floxed-only controls for each study (Tfam$^{f/f}$, Mfn1$^{f/f}$/Mfn2$^{f/f}$, or Clec16a$^{f/f}$ mice) were phenotypically indistinguishable from each other and combined as controls (Ctrl) as noted, with the exception of lineage tracing studies where controls were *Ins1*-Cre only. *Ins1*-Cre–alone were also phenotypically indistinguishable from wild-type C57BL/6N controls, consistent with previous reports from our group and others[31,32,39,110]. For inducible β-cell deletion, MIP1-CreERT mice (JAX 024709) were used or crossed to Clec16a$^{f/f}$ mice to generate iβ-Clec16a^{KO} mice as previously described[67]. To induce knockout in this model, 7 wk old mice were injected intraperitoneally with 2mg of tamoxifen (Cayman Chemicals) in corn oil every other day for 5 days. MIP1-CreERT alone mice injected with tamoxifen were used as controls for these studies. For liver specific deletion, tdTomato reporter, Tfam$^{f/f}$, and Mfn1$^{f/f}$/Mfn2$^{f/f}$ mice at 12 wk of age were injected intraperitoneally with 2x10^{11} particles of AAV-Tbg^{cre} (AAV8 serotype; Vector Biolabs; San Francisco, CA, USA) and placed on high fat diet for 6 wk. Mixed sex cohorts were used throughout the study. Mice were between 7 weeks and 1 year of age at the time of study, depending on endpoint (information

is provided in the text). Mice were randomized into treatment or vehicle control groups and/or regular chow or high fat diet groups, as necessary.

Human islet samples: All human samples were procured from de-identified donors with or without diabetes from the Integrated Islet Distribution Program, Alberta IsletCore, or Prodo Laboratories and approved by the University of Michigan Institutional Review Board. Human primary islets were cultured at 37°C with 5% CO_2 in PIM(S) media (Prodo Laboratories, Aliso Viejo, CA, USA) supplemented with 10% FBS, 100 U/mL penicillin/streptomycin, 100 U/mL antibiotic/antimycotic, and 1mM PIM(G) (Prodo Laboratories, Aliso Viejo, CA, USA). Islets were used from male and female donors, and donor information is provided in Table S2.

Mouse primary islet cultures: Mouse primary islets were isolated by perfusing pancreata with a 1 mg/mL solution of Collagenase P (Millipore Sigma; St Louis, MO, USA) in 1 X HBSS into the pancreatic duct. Following excision of the pancreas, pancreata were incubated at 37°C for 13 min, and Collagenase P was deactivated by addition of 1XHBSS + 10% adult bovine serum (Quench buffer). Pancreata were dissociated mechanically by vigorous shaking for 30 sec, the resulting cell suspension was passed through a 70 µM cell strainer (Fisher Scientific, Waltham, MA, USA). Cells were centrifuged at 1000 rpm for 2 min, the pellet was resuspended in 20 mL Quench buffer and gently vortexed to thoroughly mix. Cells were again centrifuged at 1000 rpm, 1 min. This wash step was repeated once more. Following washes, the cell pellet was resuspended in 5 mL Histopaque (Millipore-Sigma; St Louis, MO, USA) with gentle vortexing. An additional 5 mL Histopaque was layered on the cell suspension, and finally 10 mL Quench buffer was gently layered on top. The cells were spun at 900 x g for 30 min at 10°C, with the brake off. The entire Histopaque gradient was pipetted off and passed through an inverted 70 µM filter to trap the islets cells. Islets were washed twice with 10 mL Quench buffer and once with complete islet media (RPMI-1640 supplemented with 100 U/mL penicillin/streptomycin, 10% FBS, 1 mM HEPES, 2

mM L-Glutamine, 100 U/mL antibiotic/antimycotic and 10 mM sodium pyruvate). The filter was inverted into a sterile petri dish and cells were washed into the dish with 4.5 mL complete islet media. Islets were left to recover overnight, and treatments began the next day. Mouse islets were treated with ISRIB (100 nM, 24 h), Valinomycin (250 μM, 3 h), or vehicle controls, and were isolated from both male and female mice.

METHOD DETAILS

High fat diet feeding: *Ins1*-Cre or β-Clec16a^{KO} mice were randomized into 10% regular fat diet or 60% high fat diet (Research Diets Inc; New Brunswick, NJ, USA) at weaning. Access to food was *ad libitum* for 12 weeks. Mice were then subjected to *in vivo* metabolic analyses as required (detailed in following sections), and pancreatic tissue was harvested at the end of the study for immunohistochemistry, *ex vivo* islet studies, or sequencing studies.

Intraperitoneal Glucose Tolerance Tests (IPGTT): Mice were fasted for 6 h. Fasting blood glucose measurements were taken by tail nick (Bayer Contour glucometer) before an IP injection of 2 mg/kg glucose was administered. Blood glucose measurements were then taken at 15, 30, 60 and 120 mins. Following the test, mice were returned to housing cages with *ad libitum* access to food.

***In vivo* Glucose Stimulation Insulin Secretion (GSIS) test:** Mice were fasted for 6 h. Fasting blood glucose was measured after tail nick with a glucometer (Bayer Contour) and a 20 μL blood sample was collected using capillary tubes (Fisher Scientific) and stored on ice. Mice were injected with 3mg/kg glucose and blood glucose and blood samples were taken after 3 min. Blood samples were ejected from the capillary tubes into 1.5 mL tubes, spun at 16,000 x *g*, 4°C for 10 min, and serum was aliquoted to new 1.5 mL tubes. Serum insulin levels were measured by

ELISA (Alpco; Salem, NH). Following the test mice were returned to housing cages with *ad libitum* access to food.

Intraperitoneal Insulin Tolerance Tests (ITT): Mice were fasted for 6 h. Fasting blood glucose was measured after tail nick with a glucometer (Bayer Contour). Mice were injected with 0.8 U/kg insulin (Humulin R; Eli Lilly; Indianapolis, IN) and blood glucose measured at 15, 30, and 60 min. Following the test mice were returned to housing cages with *ad libitum* access to food.

Mini-osmotic pump implantation: While under inhaled isoflurane anesthesia, all mice were implanted subcutaneously with an Alzet micro-osmotic pump (model 2006, Durect, Cupertino, CA, USA) with either vehicle or phlorizin (0.8 mg/kg/d for 6 weeks) as previously described[111]. Mice were treated with meloxicam once prior to pump implantation and following implantation (5 mg/kg once daily for up to 3 days), monitored for wound healing or signs of distress, and treated with topical antibiotics (triple antibiotic ointment). Urine glucose concentrations were measured 5 weeks after pump implantation (Germaine Labs).

***In vivo* ISRIB treatment:** Mice were administered 2.5 µg/g ISRIB (ApexBio), dissolved in 40% saline;50% polyethylene glycol; 10% DMSO, or vehicle alone intraperitoneally daily for 5 weeks.

Mitophagy assessment in live human islets: Human islets from non-diabetic donors or those with T2D donors were cultured for a maximum of 48 h after shipment. On the day of the experiment islets were incubated with 100nM MTphagy dye (Dojindo Molecular Technologies; Rockville, MD, USA) for 30 min. Vehicle (DMSO) or 1mM Valinomycin (Sigma) was then added to the islets for 3 h. Islets were then dispersed to single cells using 500 µL 0.25% trypsin and incubation at 37°C for 3min. This was followed by gentle pipetting up and down approx. 10 times and neutralization of the trypsin with human islet FACS buffer (1X KRBH + 1% BSA). Single cells

were sedimented by centrifugation at room temperature, 2000 rpm, 1 min, and the pelleted cells were washed twice with 1X PBS. The cells were resuspended in 500 µL human islet FACS buffer, transferred to FACS tubes, and incubated with 500 nM Fluozin-3 and 2.5 nM TMRE for 30 min at 37°C to label insulin granule positive β cells and mitochondrial membrane potential respectively. Cells were centrifuged at 1400rpm, room temperature, 3min and resuspended in 500µL human islet FACS buffer. Samples were analyzed on an LSR Fortessa flow cytometer (BD Biosciences). Single cells were gated using forward scatter and side scatter (FSC and SSC, respectively) plots, DAPI staining was used to exclude dead cells, and Fluozin-3 was used to identify β-cells. Mtphagy measurements in β-cells were made using 488 nm excitation laser with a 710 nm emission filter and analyzed using FlowJo (Tree Star Inc.). A total of 5,000 β cells was quantified from each independent islet preparation. Representative gating strategy is displayed in Figure S11A.

Mitophagy assessment in live mouse islets using mtKeima: mtKeima-Ctrl or mtKeima-β-Clec16a^{KO} islets were isolated and treated for 24 h with vehicle (DMSO) or 100 nM ISRIB. On the day of analysis, islets were treated with ctrl (DMSO) or 250 µM Valinomycin for 3 h. Islets were dispersed to single cells using 500 µL 0.25% trypsin and incubation at 37°C for 3min followed by gentle pipetting and neutralization of the trypsin with FACS buffer (RPMI1640 phenol free + 1% BSA). Single cells were sedimented by centrifugation at room temperature, 2000 rpm, 1 min, and the pelleted cells were washed twice with 1X PBS. The cells were resuspended in 500 µL FACS buffer, transferred to FACS tubes, and incubated with 500 nM Fluozin-3AM (ThermoFisher) for 30 min at 37°C, to label Zn^{2+} enriched insulin granules in β-cells. Cells were centrifuged at 1400rpm for 3min and resuspended in 500 µL FACS buffer. Samples were analyzed on an LSR Fortessa flow cytometer (BD Biosciences). Single cells were gated using forward scatter and side scatter (FSC and SSC, respectively) plots, DAPI staining was used to exclude dead cells, and Fluozin-3 was used to identify β cells. Mitophagy measurements were made using dual laser excitation at 407 nm and 532 nm with an emission laser of 605 nm, as previously described[33],

and results were analyzed with FlowJo (Tree Star Inc). A total of 5,000 β cells were analyzed per individual experimental replicate. Representative gating strategy is displayed in Figure S11B.

mtDNA assessment in human islets: 25 human islets per donor were handpicked and washed twice with 1X PBS. Islets were pelleted and stored at -80°C until DNA extraction using the Blood/Tissue DNeasy kit (Qiagen; Germantown, MD, USA) as per manufacturer's instructions. Relative mtDNA content was quantified by qPCR using mtDNA specific primers ND1, and nuclear DNA specific primers for B2M as previously described[112]. Primer information is provided in Table S3.

mtDNA assessment in flow sorted mouse islets: Mouse islets were isolated from 4 individual control or β-Tfam^{KO} mice and left to recover overnight. The following day, islets were dispersed to single cells (as per mt-Keima FACS protocol) and sorted on a FACSAria III cell sorted (BD Biosciences). Single cells were gated using forward scatter and side scatter (FSC and SSC, respectively) plots, DAPI staining was used to exclude dead cells, and β cells were sorted from non-β cells based on high 561 nm excitation, 582 nm emission. Positive and negative cell populations were collected in 1X PBS from each mouse, spun to pellet and DNA was extracted using the Blood/Tissue DNeasy kit (Qiagen). Relative mtDNA content was quantified by qPCR using mtDNA specific primers Mt9 and Mt11, and nuclear DNA specific primers Ndufv1 Forward and Reverse[113].

β-cell mass analysis: Whole mouse pancreas was excised, weighed, and fixed in 4% paraformaldehyde for 16 h at 4°C. Samples were stored in 70% ethanol, 4°C before being embedded in paraffin and sectioned. 3 independent depths of sections, at least 50 μM apart, were dewaxed, and rehydrated and antigen retrieval was carried out using 10 mM sodium citrate (pH 6.0) in a microwave for 10 min. Sections were washed twice with 1X PBS, blocked for 1 h at room

temperature with 5% donkey serum in PBT (1X PBS, 0.1% Triton X-100, 1% BSA). Sections were then incubated in the following primary antisera overnight at 4°C in PBT: guinea pig anti-insulin (Abcam; Waltham, MA, USA), rabbit anti-glucagon (Santa Cruz; Dallas, TX, USA). Sections were then washed twice with PBS and incubated for 2 h at room temperature with species specific Cy2 and Cy3 conjugated secondary antibodies. Nuclear labelling was performed using DAPI (Molecular Probes). Sections were scanned using an Olympus IX81 microscope (Olympus; Center Valley, PA, USA) at 10X magnification, with image stitching for quantification (Olympus). β-cell mass quantification (estimated as total insulin positive area/total pancreatic area multiplied by pancreatic weight) was performed on stitched images of complete pancreatic sections from 3 independent regions.

Immunofluorescence of paraffin embedded sections: Whole mouse pancreas was excised, weighed, and fixed in 4% paraformaldehyde for 16 h at 4°C. Samples were stored in 70% ethanol at 4°C, before being embedded in paraffin and sectioned. For Aldh1a3/Pdx1 staining, antigen retrieval was carried out using 1 X HistoVT buffer (Nacalai USA Inc; San Diego, CA, USA) in an antigen retriever pressure cooker (Electron Microscopy Sciences; Hatfield, PA, USA). Sections were washed twice with 1X PBS, blocked for 1 h at room temperature with 1 X Blocking One solution (Nacalai USA Inc; San Diego, CA, USA). Sections were then incubated in the following primary antisera overnight at 4°C in 1 X PBS + 1% tween + 20% Blocking One solution: rabbit anti-Aldh1a3 (Novus Biologicals; Littleton, CO, USA). Sections were then washed twice with PBS and incubated for 2 h at room temperature with species specific Cy2 and Cy3 conjugated secondary antibodies. For Ucn3/Pdx1 staining, antigen retrieval was carried out using 10mM sodium citrate (pH 6.0) in a microwave on high for 10min. For Glut2/Pdx1 staining, antigen retrieval was carried out using 1 X R-Buffer A (Electron Microscopy Sciences; Hatfield, PA, USA) in an antigen retriever pressure cooker (Electron Microscopy Sciences; Hatfield, PA, USA). Sections were then washed twice with 1X PBS, blocked for 1 h at room temperature with 5%

donkey serum in PBT. Sections were then incubated in the following antisera overnight at 4°C in PBT: rabbit anti-Ucn3[114], or rabbit anti-Glut2 (Millipore Sigma; St Louis, MO, USA) and goat anti-Pdx1 (Abcam; Waltham, MA, USA). Sections were then washed twice with PBS and incubated for 2 h at room temperature with species specific Cy2 and Cy3 conjugated secondary antibodies. Nuclear labelling was performed using DAPI (Molecular Probes). Images were captured under 100X oil immersion magnification on an Olympus IX81 microscope. Quantification of co-positive cells was carried out by a blinded third-party researcher, and samples were re-identified after quantification to reduce bias. Antibody information is provided in Table S4.

Lineage tracing immunofluorescence analysis: Whole pancreas was excised, weighed, and fixed in 4% paraformaldehyde for 16 h before being washed with 70 % ethanol and incubated with 50% sucrose solution in PBS overnight. Pancreata were then embedded in OCT (ThermoFisher; Waltham, MA, USA) and frozen and stored at -80°C. 10 µM sections were cut using a Leica CM3050 Cryostat at -20°C, and the slides were stored at -80°C until imaging. Sections were thawed briefly, washed twice with 1X PBS, blocked with 5% donkey serum in PBT, and incubated overnight at 4°C with the following primary antisera: guinea pig anti-insulin (Abcam; Waltham, MA, USA) and rabbit anti-glucagon (Santa Cruz; Dallas, TX, USA). Sections were then washed twice with PBS and incubated for 2 h at room temperature with species specific Cy2 and Cy5 conjugated secondary antibodies, endogenous tdTomato was bright enough to capture without antibody detection. Nuclear labelling was performed using DAPI (Molecular Probes). Images were captured on a Nikon A1 Confocal microscope at 40X oil immersion magnification, z-stacks were captured to ensure quantification of single planes of cells.

Pseudoislets: Pseudoislets were prepared using the protocol described by Walker et. al.[59]. Briefly, human islets were handpicked and then dispersed with trypsin (Thermo Scientific). Islet cells were counted and incubated with adenovirus expressing shRNA against human TFAM or a

scramble control for 2 hr at MOI of 500. Cells were then seeded at 2000 cells per well in CellCarrier Spheroid Ultra-low attachment microplates (PerkinElmer) in enriched pseudoislet media as described[59]. Cells were allowed to reaggregate for 7 days before being harvested for cryosections or RNA isolation, cDNA generation, and Sybr-based qRT-PCR measurement as previously described[35]. Primer information is provided in Table S3.

Immunoblot analysis: Isolated mouse islets, human pseudoislets or frozen liver tissue was homogenized in RIPA buffer containing protease and phosphatase inhibitors. Samples were centrifuged at full speed for 10min, 4°C to pellet insoluble material and the supernatant was used for immunoblot analysis. Protein quantification was carried out using a Pierce MicroBCA kit (ThermoFisher; Waltham, MA, USA). Up to 25µg of protein lysate from islets and pseudoislets or 150 µg of protein lysate from liver were prepared in Laemmli buffer with DTT and denatured at 70°C for 10min, or 37°C for 30min for OXPHOS analysis. Samples were then run on a 4-15% Tris-glycine protein gel (Bio-Rad; Hercules, CA, USA) at 150V until separated. Samples were then transferred to a nitrocellulose membrane at 90V for 90min, membranes were blocked with 5% skim milk in 1X TBS + 0.05% Tween-20 and incubated overnight at 4°C with primary antisera. Membranes were then washed 3X with 1X TBS+0.05% Tween-20 and incubated with species-specific HRP conjugated secondary antisera (Vector Labs).

Perceval imaging: ATP/ADP ratio was monitored using the PercevalHR biosensor[63]. Islets were perfused with 16.7 mM glucose to stimulate ATP production in a recording chamber on an Olympus IX-73 inverted epifluorescence microscope (Olympus). PercevalHR was excited at 488 nm using a TILL Polychrome V monochromator (FEI), and a QuantEM:512SC cooled CCD camera (PhotoMetrics) was used to collect emission at 527 nm[115]. Data were acquired and analyzed using Metafluor (Invitrogen) and plotted using Igor Pro (WaveMetrics Inc.).

Bulk RNA-Seq of liver: Sequencing was performed by the Advanced Genomics Core at University of Michigan Medical School. Total RNA was isolated from frozen liver samples and DNase treated using commercially available kits (Omega Biotek and Ambion, respectively). Libraries were constructed and subsequently subjected to 151 bp paired-end cycles on the NovaSeq-6000 platform (Illumina). FastQC (v0.11.8) was used to ensure the quality of data. Reads were mapped to the reference genome GRCm38 (ENSEMBL), using STAR (v2.6.1b) and assigned count estimates to genes with RSEM (v1.3.1). Alignment options followed ENCODE standards for RNA-seq. FastQC was used in an additional post-alignment step to ensure that only high-quality data were used for expression quantitation and differential expression. Data were pre-filtered to remove genes with 0 counts in all samples. Differential gene expression analysis was performed using DESeq2, using a negative binomial generalized linear model (thresholds: linear fold change >1.5 or <-1.5, Benjamini-Hochberg FDR (P_{adj}) <0.05). Plots were generated using variations of DESeq2 plotting functions and other packages with Genialis (Boston, MA, USA).

Nuclear isolation from mouse islets: Isolated islets were handpicked, washed twice with PBS, and dissociated to single cells with 500 µL 0.25% trypsin at 37°C for 3min followed by vigorous pipetting and quenching with complete islet media. Single cells were washed twice with PBS and finally resuspended in 1X HBSS + 200 U/mL DNAse and incubated at 37°C for 30min. Cells were washed 4X with PBS to ensure removal of DNAse and resuspended in PBS + 1% BSA. Viability was checked using trypan blue, and only samples above 80% viability were carried forward. Cells were split evenly into 2 portions for differential snRNA and snATAC isolation protocols. For snRNA, cells were pelleted at 500 x g for 5min, 4°C, and lysed with 50 µL RNA-LB (10mM Tris-HCl pH7.4, 10mM NaCl, 3mM $MgCl_2$, and 1% NP-40 in sterile nuclease free water) by incubation on ice for 3min. Nuclei were pelleted at 500 x g for 5min, 4°C, washed in 500 µL wash buffer (1X PBS, 1% BSA and 0.2U/µL RNAse inhibitor), spun at 500 x g for 5 min, 4°C and finally responded

in 100 µL wash buffer. For snATAC, cells were pelleted at 500 x g for 5 min, 4°C and lysed in 50 µL ATAC-LB (10 mM Tris-HCl pH7.4, 10 mM NaCl, 3 mM $MgCl_2$, 0.1% NP-40, 0.1% Tween-20 and 0.01% digitonin in sterile nuclease free water) by gentle pipetting 5X and incubation on ice for 3min. 1mL ATAC-wash buffer (10 mM Tris-HCl pH7.4, 10 mM NaCl, 3 mM $MgCl_2$ and 0.1% Tween-20 in sterile nuclease free water) was added and samples spun at 500 x g for 5min, 4°C. Nuclei were resuspended in nuclei buffer (10X Genomics). After all nuclei isolation protocols, nuclei were counted, and the Advanced Genomics Core at the University of Michigan processed the samples for sequencing.

Single nucleus RNA sequencing (snRNAseq) and quantification: Approximately 14,000 single nuclei were loaded onto a 10X Genomics Chromium machine and resulting captured cells were sequenced via 10X Genomics Single Cell 3P v3 chemistry (10x Genomics, USA), yielding approximately 7k nuclei per lane. All libraries were analyzed using the Cell Ranger analysis pipeline version 3.0. Briefly, reads were aligned to mouse reference sequence mm10 and unique molecular identifiers (UMIs) were quantified using the Cell Ranger "count" software with default parameters. Count data from each single nucleus were normalized to the same sequencing depth and then aggregated using the "cellranger aggr" tool. Cell barcodes with fewer than 1000 detected genes and a total mitochondrial content >20% (signifying potential apoptotic cells) were discarded from analyses.

Single nucleus ATAC sequencing (snATACseq) and quantification: Approximately 14,000 single nuclei were loaded and sequenced via 10X Genomics Single Cell ATAC v1 chemistry (10x Genomics, USA), yielding approximately 7K cells per lane. All libraries were sequenced individually on Illumina NovaSeq S4 flowcells and were analyzed using the Cell Ranger ATAC analysis pipeline version 1.2.0. Reads were similarly aligned to mouse reference sequence mm10 and fragments, open chromatin peaks were quantified using the Cell Ranger ATAC "count"

software with default parameters. Fragment data from each single cell library were normalized to the same sequencing depth and then aggregated using the “cellranger aggr” tool. Resultant genomic alignment (BAM) files were filtered to contain only nucleosome free reads (<147 bp) using SAMtools version 1.8[116].

snRNAseq doublet cell detection and removal: To identify and remove potential multiplet droplets from snRNA-seq data, we used DoubletFinder[117] and Scrublet[118] to identify multiplet nuclei in an unbiased/non-cell type specific manner. For both methods, we assumed an expected doublet rate of 10% of total cells. Afterwards, we removed all multiplet nuclei identified by at least one of these two methods (union set of doublets).

snRNAseq cell clustering: Nuclei were clustered using top 2000 most variable genes, which are determined by fitting a line to the relationship of the variance and mean using a local polynomial regression (loess). Gene expression values were standardized using the observed normalized mean and expected variance (given by the fitted line). Feature variance was then calculated on the standardized values after clipping to a maximum of the square root of the number of cells. After scaling and centering the feature values, principal component analysis (PCA) was performed on the top 2000 variable features. Following this, uniform manifold approximation and projection (UMAP) was applied on the top 20 principal components to reduce the data to two dimensions. Next, a shared nearest neighbor (SNN) graph was created by calculating the neighborhood (Jaccard index) overlap between each cell and its 20 (default) nearest neighbors. To identify cell clusters, a SNN modularity optimization-based clustering algorithm was used[119].

Annotation of cell types in snRNAseq: Islet cell clusters were annotated based on expression of known cell-type markers —*Ins1/2* (beta), *Gcg* (alpha), *Sst* (delta). The remaining cells were

annotated using pathway databases and annotations from the *clusterProfiler* (version 3.14.0[120]) R package.

Differential gene expression analysis: Differential expression analyses was performed using the FindMarkers function (with default parameters) and the wilcox test option in the R package Seurat[119] to identify genes that are enriched in each cell type. In each comparison, protein coding genes and long intergenic non-coding RNAs (lincRNAs) with one or more UMIs in at least 10% of either cell type population being compared was used. Differentially expressed genes with FDR < 5% were regarded as significant results.

Pathway analysis of differentially expressed genes: Differentially expressed genes for each cell-type were functionally annotated using the R package *clusterProfiler* (version 3.14.0[120]). The Kyoto Encyclopedia of Genes and Genomes (KEGG), gene ontology (GO), and WikiPathways databases were used to determine associations with particular biological processes, diseases, and molecular functions. The top pathways with an FDR-adjusted p-value <5% were summarized in the results.

Integration of snRNA-seq and snATAC-seq data: Integrative clustering and analysis of single nuclei transcriptomes and single nucleus epigenomes was performed using the R package Seurat[119]. First, gene activity scores were derived from the resultant snATAC-seq peak count-matrix using the CreateGeneActivityMatrix function with default parameters. Next, single nuclei with < 5,000 total read counts were discarded from analyses. The resultant single nuclei and gene activity scores were log normalized and scaled. Using the processed snRNA-seq data (also analyzed with Seurat), we identified anchors between the snATAC-seq gene activity score matrix and snRNA-seq gene expression matrix following the methodology described in [119]. After identifying anchors between the datasets, cell-type labels from the snRNA-seq dataset were

transferred to the snATAC-seq dataset and a prediction and confidence score was assigned for each cell.

Aggregation of single nucleus ATAC-seq profiles into pseudo-bulk profiles: For each cell-type, single nucleus ATAC-seq profiles were aggregated into single bulk ATAC-seq profiles using using SAMtools version 1.8[116] and the "merge" command. Merged BAM files were sorted and indexed using SAMtools and provided as input to identify open chromatin peaks. Peaks were called using MACS version 2.1.0.20151222 and the following parameters "-g 'mm' --nomodel --call-summits --qval 0.01 --keep-dup all -B -f BAMPE". Cell-type specific open chromatin peaks were identified using BEDtools version 2.27.0[121] and the "bedtools intersect -v" command.

Transcription factor motif enrichment analysis: The *findMotifsGenome.pl* (HOMER version 4.6[68]) script with parameters "hg19 -size 200" was used to determine TF motifs enriched in ATAC-seq peaks for KO beta cells relative to control beta cells (and vice versa). As an example, to identify TF motifs enriched in KO beta cell-specific peaks, we provided these peaks as the foreground, and the control beta cell-specific peaks as the background.

Statistics

In all figures, data are presented as means ± SEM, and error bars denote SEM, unless otherwise noted in the legends. Statistical comparisons were performed using unpaired two-tailed Student's t-tests, one-way or two-way ANOVA, followed by Tukey's or Sidak's post-hoc test for multiple comparisons, as appropriate (GraphPad Prism). A P value < 0.05 was considered significant.

Acknowledgements

S.A.S. was supported by the JDRF (CDA-2016-189, COE-2019-861), the NIH (R01 DK108921, U01 DK127747), the Department of Veterans Affairs (I01 BX004444), the Brehm family, and the

Anthony family. G.L.P. was supported by the American Diabetes Association (19-PDF-063). B.A.K. was supported by the Department of Veterans Affairs (I01 BX004444). L.S.S. was supported by the NIH (R01 DK46409). The JDRF Career Development Award to S.A.S. is partly supported by the Danish Diabetes Academy and the Novo Nordisk Foundation. We acknowledge the Microscopy, Imaging and Cellular Physiology Core and Islet Core of the University of Michigan DRC (P30 DK020572) for assistance with imaging studies and pseudoislet studies, respectively. We thank the University of Michigan Flow Cytometry Core for assistance with flow cytometry studies. Next generation sequencing was carried out in the Advanced Genomics Core at the University of Michigan. We thank Dr. K. Claiborn and members of the Soleimanpour laboratory for helpful advice. Human pancreatic islets and/or other resources were provided by the NIDDK-funded Integrated Islet Distribution Program (IIDP) (RRID:SCR _014387) at City of Hope, NIH Grant # U24DK098085.

Author Contributions

G.L.P. and E.M.W. conceived, designed, and performed experiments, interpreted results, drafted and reviewed the manuscript. N.L. designed and performed experiments, interpreted results, and reviewed the manuscript. A.L., V.S., J.Z., T.S., E.C.R., A.R., K.M., V.S.P., I.X.Z., B.T., D.Z., S.A.W., and L.H. designed and performed experiments and interpreted results. S.C.J.P., P.A., L.Y., B.A.K., L.S.S., and L.S. designed studies, interpreted results, and reviewed the manuscript. M.L.S. designed studies, interpreted results, edited, and reviewed the manuscript. S.A.S. conceived and designed the studies, interpreted results, drafted, edited, and reviewed the manuscript.

Conflict of interest statement

The authors have declared that no conflict of interest exists.

REFERENCES

1 Lowell, B. B. & Shulman, G. I. Mitochondrial dysfunction and type 2 diabetes. *Science* **307**, 384-387, doi:10.1126/science.1104343 (2005).

2 Anello, M. *et al.* Functional and morphological alterations of mitochondria in pancreatic beta cells from type 2 diabetic patients. *Diabetologia* **48**, 282-289, doi:10.1007/s00125-004-1627-9 (2005).

3 Masini, M. *et al.* Ultrastructural alterations of pancreatic beta cells in human diabetes mellitus. *Diabetes Metab Res Rev* **33**, doi:10.1002/dmrr.2894 (2017).

4 Stump, C. S., Short, K. R., Bigelow, M. L., Schimke, J. M. & Nair, K. S. Effect of insulin on human skeletal muscle mitochondrial ATP production, protein synthesis, and mRNA transcripts. *Proc Natl Acad Sci U S A* **100**, 7996-8001, doi:10.1073/pnas.1332551100 (2003).

5 Asmann, Y. W. *et al.* Skeletal muscle mitochondrial functions, mitochondrial DNA copy numbers, and gene transcript profiles in type 2 diabetic and nondiabetic subjects at equal levels of low or high insulin and euglycemia. *Diabetes* **55**, 3309-3319, doi:10.2337/db05-1230 (2006).

6 Phielix, E. *et al.* Lower intrinsic ADP-stimulated mitochondrial respiration underlies in vivo mitochondrial dysfunction in muscle of male type 2 diabetic patients. *Diabetes* **57**, 2943-2949, doi:10.2337/db08-0391 (2008).

7 Ritov, V. B. *et al.* Deficiency of subsarcolemmal mitochondria in obesity and type 2 diabetes. *Diabetes* **54**, 8-14, doi:10.2337/diabetes.54.1.8 (2005).

8 Koliaki, C. *et al.* Adaptation of hepatic mitochondrial function in humans with non-alcoholic fatty liver is lost in steatohepatitis. *Cell Metab* **21**, 739-746, doi:10.1016/j.cmet.2015.04.004 (2015).

9 Schmid, A. I. *et al.* Liver ATP synthesis is lower and relates to insulin sensitivity in patients with type 2 diabetes. *Diabetes Care* **34**, 448-453, doi:10.2337/dc10-1076 (2011).

10 Szendroedi, J. *et al.* Abnormal hepatic energy homeostasis in type 2 diabetes. *Hepatology* **50**, 1079-1086, doi:10.1002/hep.23093 (2009).

11 Kotronen, A., Juurinen, L., Tiikkainen, M., Vehkavaara, S. & Yki-Jarvinen, H. Increased liver fat, impaired insulin clearance, and hepatic and adipose tissue insulin resistance in type 2 diabetes. *Gastroenterology* **135**, 122-130, doi:10.1053/j.gastro.2008.03.021 (2008).

12 Pinti, M. V. *et al.* Mitochondrial dysfunction in type 2 diabetes mellitus: an organ-based analysis. *Am J Physiol Endocrinol Metab* **316**, E268-E285, doi:10.1152/ajpendo.00314.2018 (2019).

13 Wigger, L. *et al.* Multi-omics profiling of living human pancreatic islet donors reveals heterogeneous beta cell trajectories towards type 2 diabetes. *Nat Metab* **3**, 1017-1031, doi:10.1038/s42255-021-00420-9 (2021).

14 Koeck, T. *et al.* A common variant in TFB1M is associated with reduced insulin secretion and increased future risk of type 2 diabetes. *Cell Metab* **13**, 80-91, doi:10.1016/j.cmet.2010.12.007 (2011).

15 Sangwung, P., Petersen, K. F., Shulman, G. I. & Knowles, J. W. Mitochondrial Dysfunction, Insulin Resistance, and Potential Genetic Implications. *Endocrinology* **161**, doi:10.1210/endocr/bqaa017 (2020).

16 Palmer, C. J. *et al.* Cdkal1, a type 2 diabetes susceptibility gene, regulates mitochondrial function in adipose tissue. *Mol Metab* **6**, 1212-1225, doi:10.1016/j.molmet.2017.07.013 (2017).

17 Kraja, A. T. *et al.* Associations of Mitochondrial and Nuclear Mitochondrial Variants and Genes with Seven Metabolic Traits. *Am J Hum Genet* **104**, 112-138, doi:10.1016/j.ajhg.2018.12.001 (2019).

18 Mercader, J. M. *et al.* Identification of novel type 2 diabetes candidate genes involved in the crosstalk between the mitochondrial and the insulin signaling systems. *PLoS Genet* **8**, e1003046, doi:10.1371/journal.pgen.1003046 (2012).
19 Yonova-Doing, E. *et al.* An atlas of mitochondrial DNA genotype-phenotype associations in the UK Biobank. *Nat Genet* **53**, 982-993, doi:10.1038/s41588-021-00868-1 (2021).
20 Sachdeva, M. M. & Stoffers, D. A. Minireview: Meeting the demand for insulin: molecular mechanisms of adaptive postnatal beta-cell mass expansion. *Mol Endocrinol* **23**, 747-758, doi:10.1210/me.2008-0400 (2009).
21 Cinti, F. *et al.* Evidence of beta-Cell Dedifferentiation in Human Type 2 Diabetes. *J Clin Endocrinol Metab* **101**, 1044-1054, doi:10.1210/jc.2015-2860 (2016).
22 Talchai, C., Xuan, S., Lin, H. V., Sussel, L. & Accili, D. Pancreatic beta cell dedifferentiation as a mechanism of diabetic beta cell failure. *Cell* **150**, 1223-1234, doi:10.1016/j.cell.2012.07.029 (2012).
23 Wang, Z., York, N. W., Nichols, C. G. & Remedi, M. S. Pancreatic beta cell dedifferentiation in diabetes and redifferentiation following insulin therapy. *Cell Metab* **19**, 872-882, doi:10.1016/j.cmet.2014.03.010 (2014).
24 Kahn, C. R., Wang, G. & Lee, K. Y. Altered adipose tissue and adipocyte function in the pathogenesis of metabolic syndrome. *J Clin Invest* **129**, 3990-4000, doi:10.1172/JCI129187 (2019).
25 Moretto, P. *et al.* Regulation of hyaluronan synthesis in vascular diseases and diabetes. *J Diabetes Res* **2015**, 167283, doi:10.1155/2015/167283 (2015).
26 Ikeda, S. *et al.* Yes-Associated Protein (YAP) Facilitates Pressure Overload-Induced Dysfunction in the Diabetic Heart. *JACC Basic Transl Sci* **4**, 611-622, doi:10.1016/j.jacbts.2019.05.006 (2019).
27 Westermann, B. Mitochondrial fusion and fission in cell life and death. *Nat Rev Mol Cell Biol* **11**, 872-884, doi:10.1038/nrm3013 (2010).
28 Kaufman, B. A., Li, C. & Soleimanpour, S. A. Mitochondrial regulation of beta-cell function: maintaining the momentum for insulin release. *Mol Aspects Med* **42**, 91-104, doi:10.1016/j.mam.2015.01.004 (2015).
29 Lawlor, N. *et al.* Single-cell transcriptomes identify human islet cell signatures and reveal cell-type-specific expression changes in type 2 diabetes. *Genome Res* **27**, 208-222, doi:10.1101/gr.212720.116 (2017).
30 Gingerich, M. A. *et al.* An intrinsically disordered protein region encoded by the human disease gene CLEC16A regulates mitophagy. *Autophagy*, 1-19, doi:10.1080/15548627.2022.2080383 (2022).
31 Sidarala, V. *et al.* Mitofusin 1 and 2 regulation of mitochondrial DNA content is a critical determinant of glucose homeostasis. *Nat Commun* **13**, 2340, doi:10.1038/s41467-022-29945-7 (2022).
32 Sidarala, V. *et al.* Mitophagy protects beta cells from inflammatory damage in diabetes. *JCI Insight* **5**, doi:10.1172/jci.insight.141138 (2020).
33 Sun, N. *et al.* Measuring In Vivo Mitophagy. *Mol Cell* **60**, 685-696, doi:10.1016/j.molcel.2015.10.009 (2015).
34 Sun, N. *et al.* A fluorescence-based imaging method to measure in vitro and in vivo mitophagy using mt-Keima. *Nat Protoc* **12**, 1576-1587, doi:10.1038/nprot.2017.060 (2017).
35 Soleimanpour, S. A. *et al.* The diabetes susceptibility gene Clec16a regulates mitophagy. *Cell* **157**, 1577-1590, doi:10.1016/j.cell.2014.05.016 (2014).
36 Soleimanpour, S. A. *et al.* Diabetes Susceptibility Genes Pdx1 and Clec16a Function in a Pathway Regulating Mitophagy in beta-Cells. *Diabetes* **64**, 3475-3484, doi:10.2337/db15-0376 (2015).

37 Gunton, J. E. *et al.* Loss of ARNT/HIF1beta mediates altered gene expression and pancreatic-islet dysfunction in human type 2 diabetes. *Cell* **122**, 337-349, doi:10.1016/j.cell.2005.05.027 (2005).
38 Stoffers, D. A., Stanojevic, V. & Habener, J. F. Insulin promoter factor-1 gene mutation linked to early-onset type 2 diabetes mellitus directs expression of a dominant negative isoprotein. *J Clin Invest* **102**, 232-241, doi:10.1172/JCI2242 (1998).
39 Thorens, B. *et al.* Ins1(Cre) knock-in mice for beta cell-specific gene recombination. *Diabetologia* **58**, 558-565, doi:10.1007/s00125-014-3468-5 (2015).
40 Zhu, M. *et al.* beta cell aging and age-related diabetes. *Aging (Albany NY)* **13**, 7691-7706, doi:10.18632/aging.202593 (2021).
41 Silva, J. P. *et al.* Impaired insulin secretion and beta-cell loss in tissue-specific knockout mice with mitochondrial diabetes. *Nat Genet* **26**, 336-340, doi:10.1038/81649 (2000).
42 Magnuson, M. A. & Osipovich, A. B. Pancreas-specific Cre driver lines and considerations for their prudent use. *Cell Metab* **18**, 9-20, doi:10.1016/j.cmet.2013.06.011 (2013).
43 Madisen, L. *et al.* A robust and high-throughput Cre reporting and characterization system for the whole mouse brain. *Nature neuroscience* **13**, 133-140, doi:10.1038/nn.2467 (2010).
44 Qiu, W. L. *et al.* Deciphering Pancreatic Islet beta Cell and alpha Cell Maturation Pathways and Characteristic Features at the Single-Cell Level. *Cell Metab* **25**, 1194-1205 e1194, doi:10.1016/j.cmet.2017.04.003 (2017).
45 Hua, H. & Sarvetnick, N. Expression of Id1 in adult, regenerating and developing pancreas. *Endocrine* **32**, 280-286, doi:10.1007/s12020-008-9036-3 (2007).
46 Hua, H. *et al.* BMP4 regulates pancreatic progenitor cell expansion through Id2. *J Biol Chem* **281**, 13574-13580, doi:10.1074/jbc.M600526200 (2006).
47 Ghil, S. H., Jeon, Y. J. & Suh-Kim, H. Inhibition of BETA2/NeuroD by Id2. *Exp Mol Med* **34**, 367-373, doi:10.1038/emm.2002.52 (2002).
48 Lorberbaum, D. S. & Sussel, L. A Notch in Time: Spatiotemporal Analysis of Notch Signaling during Pancreas Development. *Dev Cell* **52**, 681-682, doi:10.1016/j.devcel.2020.02.018 (2020).
49 Namwanje, M. & Brown, C. W. Activins and Inhibins: Roles in Development, Physiology, and Disease. *Cold Spring Harb Perspect Biol* **8**, doi:10.1101/cshperspect.a021881 (2016).
50 Gere-Becker, M. B., Pommerenke, C., Lingner, T. & Pieler, T. Retinoic acid-induced expression of Hnf1b and Fzd4 is required for pancreas development in Xenopus laevis. *Development* **145**, doi:10.1242/dev.161372 (2018).
51 Georgiadou, E. *et al.* Mitofusins Mfn1 and Mfn2 Are Required to Preserve Glucose- but Not Incretin-Stimulated beta-Cell Connectivity and Insulin Secretion. *Diabetes* **71**, 1472-1489, doi:10.2337/db21-0800 (2022).
52 Kim-Muller, J. Y. *et al.* Aldehyde dehydrogenase 1a3 defines a subset of failing pancreatic beta cells in diabetic mice. *Nat Commun* **7**, 12631, doi:10.1038/ncomms12631 (2016).
53 Gutierrez, G. D. *et al.* Pancreatic beta cell identity requires continual repression of non-beta cell programs. *J Clin Invest* **127**, 244-259, doi:10.1172/JCI88017 (2017).
54 Szklarczyk, D. *et al.* The STRING database in 2021: customizable protein-protein networks, and functional characterization of user-uploaded gene/measurement sets. *Nucleic Acids Res* **49**, D605-D612, doi:10.1093/nar/gkaa1074 (2021).
55 Gauthier, B. R. *et al.* PDX1 deficiency causes mitochondrial dysfunction and defective insulin secretion through TFAM suppression. *Cell Metab* **10**, 110-118, doi:10.1016/j.cmet.2009.07.002 (2009).
56 Quiros, P. M., Mottis, A. & Auwerx, J. Mitonuclear communication in homeostasis and stress. *Nat Rev Mol Cell Biol* **17**, 213-226, doi:10.1038/nrm.2016.23 (2016).

57 Quiros, P. M. *et al.* Multi-omics analysis identifies ATF4 as a key regulator of the mitochondrial stress response in mammals. *J Cell Biol* **216**, 2027-2045, doi:10.1083/jcb.201702058 (2017).
58 Chen, J., Fontes, G., Saxena, G., Poitout, V. & Shalev, A. Lack of TXNIP protects against mitochondria-mediated apoptosis but not against fatty acid-induced ER stress-mediated beta-cell death. *Diabetes* **59**, 440-447, doi:10.2337/db09-0949 (2010).
59 Walker, J. T. *et al.* Integrated human pseudoislet system and microfluidic platform demonstrate differences in GPCR signaling in islet cells. *JCI Insight* **5**, doi:10.1172/jci.insight.137017 (2020).
60 Evstafieva, A. G. *et al.* A sustained deficiency of mitochondrial respiratory complex III induces an apoptotic cell death through the p53-mediated inhibition of pro-survival activities of the activating transcription factor 4. *Cell Death Dis* **5**, e1511, doi:10.1038/cddis.2014.469 (2014).
61 Martinez-Reyes, I., Sanchez-Arago, M. & Cuezva, J. M. AMPK and GCN2-ATF4 signal the repression of mitochondria in colon cancer cells. *Biochem J* **444**, 249-259, doi:10.1042/BJ20111829 (2012).
62 Silva, J. M., Wong, A., Carelli, V. & Cortopassi, G. A. Inhibition of mitochondrial function induces an integrated stress response in oligodendroglia. *Neurobiol Dis* **34**, 357-365, doi:10.1016/j.nbd.2009.02.005 (2009).
63 Berg, J., Hung, Y. P. & Yellen, G. A genetically encoded fluorescent reporter of ATP:ADP ratio. *Nat Methods* **6**, 161-166, doi:10.1038/nmeth.1288 (2009).
64 Dai, D. F. *et al.* Mitochondrial oxidative stress mediates angiotensin II-induced cardiac hypertrophy and Galphaq overexpression-induced heart failure. *Circulation research* **108**, 837-846, doi:10.1161/CIRCRESAHA.110.232306 (2011).
65 Gurgul, E., Lortz, S., Tiedge, M., Jorns, A. & Lenzen, S. Mitochondrial catalase overexpression protects insulin-producing cells against toxicity of reactive oxygen species and proinflammatory cytokines. *Diabetes* **53**, 2271-2280, doi:10.2337/diabetes.53.9.2271 (2004).
66 McLean, C. Y. *et al.* GREAT improves functional interpretation of cis-regulatory regions. *Nat Biotechnol* **28**, 495-501, doi:10.1038/nbt.1630 (2010).
67 Pearson, G. *et al.* Clec16a, Nrdp1, and USP8 Form a Ubiquitin-Dependent Tripartite Complex That Regulates beta-Cell Mitophagy. *Diabetes* **67**, 265-277, doi:10.2337/db17-0321 (2018).
68 Heinz, S. *et al.* Simple combinations of lineage-determining transcription factors prime cis-regulatory elements required for macrophage and B cell identities. *Mol Cell* **38**, 576-589, doi:10.1016/j.molcel.2010.05.004 (2010).
69 Son, J. *et al.* BACH2 inhibition reverses beta cell failure in type 2 diabetes models. *J Clin Invest* **131**, doi:10.1172/JCI153876 (2021).
70 Gu, C. *et al.* Pancreatic beta cells require NeuroD to achieve and maintain functional maturity. *Cell Metab* **11**, 298-310, doi:10.1016/j.cmet.2010.03.006 (2010).
71 Chen, H., Walker, G. E., Taylor, S. I. & McKeon, C. Proximal enhancer of the human insulin receptor gene binds the transcription factor Sp1. *Diabetes* **43**, 884-889, doi:10.2337/diab.43.7.884 (1994).
72 DHAWAN, S., GURLO, T. & WANG, J. K. 259-OR: Epigenetic Coregulation of Beta-Cell Function and Survival in Postnatal Life. *Diabetes* **69**, doi:10.2337/db20-259-OR (2020).
73 Li, T. *et al.* Multi-stage analysis of gene expression and transcription regulation in C57/B6 mouse liver development. *Genomics* **93**, 235-242, doi:10.1016/j.ygeno.2008.10.006 (2009).
74 Chouchani, E. T. & Kajimura, S. Metabolic adaptation and maladaptation in adipose tissue. *Nat Metab* **1**, 189-200, doi:10.1038/s42255-018-0021-8 (2019).

75 Sustarsic, E. G. *et al.* Cardiolipin Synthesis in Brown and Beige Fat Mitochondria Is Essential for Systemic Energy Homeostasis. *Cell Metab* **28**, 159-174 e111, doi:10.1016/j.cmet.2018.05.003 (2018).
76 Teresak, P. *et al.* Regulation of PRKN-independent mitophagy. *Autophagy* **18**, 24-39, doi:10.1080/15548627.2021.1888244 (2022).
77 Claypool, S. M. & Koehler, C. M. The complexity of cardiolipin in health and disease. *Trends Biochem Sci* **37**, 32-41, doi:10.1016/j.tibs.2011.09.003 (2012).
78 Perdikari, A. *et al.* BATLAS: Deconvoluting Brown Adipose Tissue. *Cell Rep* **25**, 784-797 e784, doi:10.1016/j.celrep.2018.09.044 (2018).
79 Costa-Mattioli, M. & Walter, P. The integrated stress response: From mechanism to disease. *Science* **368**, doi:10.1126/science.aat5314 (2020).
80 Halliday, M. *et al.* Partial restoration of protein synthesis rates by the small molecule ISRIB prevents neurodegeneration without pancreatic toxicity. *Cell Death Dis* **6**, e1672, doi:10.1038/cddis.2015.49 (2015).
81 Liao, X. & Butow, R. A. RTG1 and RTG2: two yeast genes required for a novel path of communication from mitochondria to the nucleus. *Cell* **72**, 61-71, doi:10.1016/0092-8674(93)90050-z (1993).
82 Liu, Z. & Butow, R. A. A transcriptional switch in the expression of yeast tricarboxylic acid cycle genes in response to a reduction or loss of respiratory function. *Mol Cell Biol* **19**, 6720-6728, doi:10.1128/MCB.19.10.6720 (1999).
83 Liu, Z. & Butow, R. A. Mitochondrial retrograde signaling. *Annu Rev Genet* **40**, 159-185, doi:10.1146/annurev.genet.40.110405.090613 (2006).
84 Pagliarini, D. J. *et al.* A mitochondrial protein compendium elucidates complex I disease biology. *Cell* **134**, 112-123, doi:10.1016/j.cell.2008.06.016 (2008).
85 Jazwinski, S. M. The retrograde response: when mitochondrial quality control is not enough. *Biochim Biophys Acta* **1833**, 400-409, doi:10.1016/j.bbamcr.2012.02.010 (2013).
86 Seale, P. *et al.* Transcriptional control of brown fat determination by PRDM16. *Cell Metab* **6**, 38-54, doi:10.1016/j.cmet.2007.06.001 (2007).
87 Uldry, M. *et al.* Complementary action of the PGC-1 coactivators in mitochondrial biogenesis and brown fat differentiation. *Cell Metab* **3**, 333-341, doi:10.1016/j.cmet.2006.04.002 (2006).
88 Jerome, M. S., Kuthethur, R., Kabekkodu, S. P. & Chakrabarty, S. Regulation of mitochondrial function by forkhead transcription factors. *Biochimie* **198**, 96-108, doi:10.1016/j.biochi.2022.03.013 (2022).
89 Vernier, M. & Giguere, V. Aging, senescence and mitochondria: the PGC-1/ERR axis. *J Mol Endocrinol* **66**, R1-R14, doi:10.1530/JME-20-0196 (2021).
90 Yoshihara, E. *et al.* ERRgamma Is Required for the Metabolic Maturation of Therapeutically Functional Glucose-Responsive beta Cells. *Cell Metab* **23**, 622-634, doi:10.1016/j.cmet.2016.03.005 (2016).
91 Fan, J. *et al.* Cyb5r3 links FoxO1-dependent mitochondrial dysfunction with beta-cell failure. *Mol Metab* **34**, 97-111, doi:10.1016/j.molmet.2019.12.008 (2020).
92 Siendones, E. *et al.* Membrane-bound CYB5R3 is a common effector of nutritional and oxidative stress response through FOXO3a and Nrf2. *Antioxid Redox Signal* **21**, 1708-1725, doi:10.1089/ars.2013.5479 (2014).
93 Nakae, J. *et al.* Forkhead transcription factor FoxO1 in adipose tissue regulates energy storage and expenditure. *Diabetes* **57**, 563-576, doi:10.2337/db07-0698 (2008).
94 Tikhanovich, I., Cox, J. & Weinman, S. A. Forkhead box class O transcription factors in liver function and disease. *J Gastroenterol Hepatol* **28 Suppl 1**, 125-131, doi:10.1111/jgh.12021 (2013).
95 Rui, L. Energy metabolism in the liver. *Compr Physiol* **4**, 177-197, doi:10.1002/cphy.c130024 (2014).

96 Huang, P. I. *et al.* PGC-1alpha mediates differentiation of mesenchymal stem cells to brown adipose cells. *J Atheroscler Thromb* **18**, 966-980, doi:10.5551/jat.7401 (2011).
97 Huang, P. I. *et al.* Enhanced differentiation of three-gene-reprogrammed induced pluripotent stem cells into adipocytes via adenoviral-mediated PGC-1alpha overexpression. *Int J Mol Sci* **12**, 7554-7568, doi:10.3390/ijms12117554 (2011).
98 Oropeza, D. *et al.* PGC-1 coactivators in beta-cells regulate lipid metabolism and are essential for insulin secretion coupled to fatty acids. *Mol Metab* **4**, 811-822, doi:10.1016/j.molmet.2015.08.001 (2015).
99 Misra, J., Kim, D. K. & Choi, H. S. ERRgamma: a Junior Orphan with a Senior Role in Metabolism. *Trends Endocrinol Metab* **28**, 261-272, doi:10.1016/j.tem.2016.12.005 (2017).
100 Ahmadian, M. *et al.* ERRgamma Preserves Brown Fat Innate Thermogenic Activity. *Cell Rep* **22**, 2849-2859, doi:10.1016/j.celrep.2018.02.061 (2018).
101 Shan, J., Fu, L., Balasubramanian, M. N., Anthony, T. & Kilberg, M. S. ATF4-dependent regulation of the JMJD3 gene during amino acid deprivation can be rescued in Atf4-deficient cells by inhibition of deacetylation. *J Biol Chem* **287**, 36393-36403, doi:10.1074/jbc.M112.399600 (2012).
102 Campbell, S. L. & Wellen, K. E. Metabolic Signaling to the Nucleus in Cancer. *Mol Cell* **71**, 398-408, doi:10.1016/j.molcel.2018.07.015 (2018).
103 Zhang, G., Wang, X., Rothermel, B. A., Lavandero, S. & Wang, Z. V. The integrated stress response in ischemic diseases. *Cell Death Differ* **29**, 750-757, doi:10.1038/s41418-021-00889-7 (2022).
104 Shrestha, N., De Franco, E., Arvan, P. & Cnop, M. Pathological beta-Cell Endoplasmic Reticulum Stress in Type 2 Diabetes: Current Evidence. *Front Endocrinol (Lausanne)* **12**, 650158, doi:10.3389/fendo.2021.650158 (2021).
105 Kahn, S. E., Hull, R. L. & Utzschneider, K. M. Mechanisms linking obesity to insulin resistance and type 2 diabetes. *Nature* **444**, 840-846, doi:10.1038/nature05482 (2006).
106 Guo, S. *et al.* Inactivation of specific beta cell transcription factors in type 2 diabetes. *J Clin Invest* **123**, 3305-3316, doi:10.1172/JCI65390 (2013).
107 Chung, K. W. *et al.* Mitochondrial Damage and Activation of the STING Pathway Lead to Renal Inflammation and Fibrosis. *Cell Metab* **30**, 784-799 e785, doi:10.1016/j.cmet.2019.08.003 (2019).
108 Engin, F. *et al.* Restoration of the unfolded protein response in pancreatic beta cells protects mice against type 1 diabetes. *Sci Transl Med* **5**, 211ra156, doi:10.1126/scitranslmed.3006534 (2013).
109 Lee, H. *et al.* Beta Cell Dedifferentiation Induced by IRE1alpha Deletion Prevents Type 1 Diabetes. *Cell Metab* **31**, 822-836 e825, doi:10.1016/j.cmet.2020.03.002 (2020).
110 Corsa, C. A. S. *et al.* The E3 ubiquitin ligase parkin is dispensable for metabolic homeostasis in murine pancreatic beta cells and adipocytes. *J Biol Chem* **294**, 7296-7307, doi:10.1074/jbc.RA118.006763 (2019).
111 Alejandro, E. U. *et al.* Disruption of O-linked N-Acetylglucosamine Signaling Induces ER Stress and beta Cell Failure. *Cell Rep* **13**, 2527-2538, doi:10.1016/j.celrep.2015.11.020 (2015).
112 Belmonte, F. R. *et al.* Digital PCR methods improve detection sensitivity and measurement precision of low abundance mtDNA deletions. *Sci Rep* **6**, 25186, doi:10.1038/srep25186 (2016).
113 Kolesar, J. E., Wang, C. Y., Taguchi, Y. V., Chou, S. H. & Kaufman, B. A. Two-dimensional intact mitochondrial DNA agarose electrophoresis reveals the structural complexity of the mammalian mitochondrial genome. *Nucleic Acids Res* **41**, e58, doi:10.1093/nar/gks1324 (2013).

114 van der Meulen, T. *et al.* Urocortin 3 marks mature human primary and embryonic stem cell-derived pancreatic alpha and beta cells. *PLoS One* **7**, e52181, doi:10.1371/journal.pone.0052181 (2012).
115 Hodson, D. J. *et al.* Incretin-modulated beta cell energetics in intact islets of Langerhans. *Mol Endocrinol* **28**, 860-871, doi:10.1210/me.2014-1038 (2014).
116 Li, H. *et al.* The Sequence Alignment/Map format and SAMtools. *Bioinformatics* **25**, 2078-2079, doi:10.1093/bioinformatics/btp352 (2009).
117 McGinnis, C. S., Murrow, L. M. & Gartner, Z. J. DoubletFinder: Doublet Detection in Single-Cell RNA Sequencing Data Using Artificial Nearest Neighbors. *Cell Syst* **8**, 329-337 e324, doi:10.1016/j.cels.2019.03.003 (2019).
118 Wolock, S. L., Lopez, R. & Klein, A. M. Scrublet: Computational Identification of Cell Doublets in Single-Cell Transcriptomic Data. *Cell Syst* **8**, 281-291 e289, doi:10.1016/j.cels.2018.11.005 (2019).
119 Butler, A., Hoffman, P., Smibert, P., Papalexi, E. & Satija, R. Integrating single-cell transcriptomic data across different conditions, technologies, and species. *Nat Biotechnol* **36**, 411-420, doi:10.1038/nbt.4096 (2018).
120 Yu, G., Wang, L. G., Han, Y. & He, Q. Y. clusterProfiler: an R package for comparing biological themes among gene clusters. *OMICS* **16**, 284-287, doi:10.1089/omi.2011.0118 (2012).
121 Quinlan, A. R. & Hall, I. M. BEDTools: a flexible suite of utilities for comparing genomic features. *Bioinformatics* **26**, 841-842, doi:10.1093/bioinformatics/btq033 (2010).

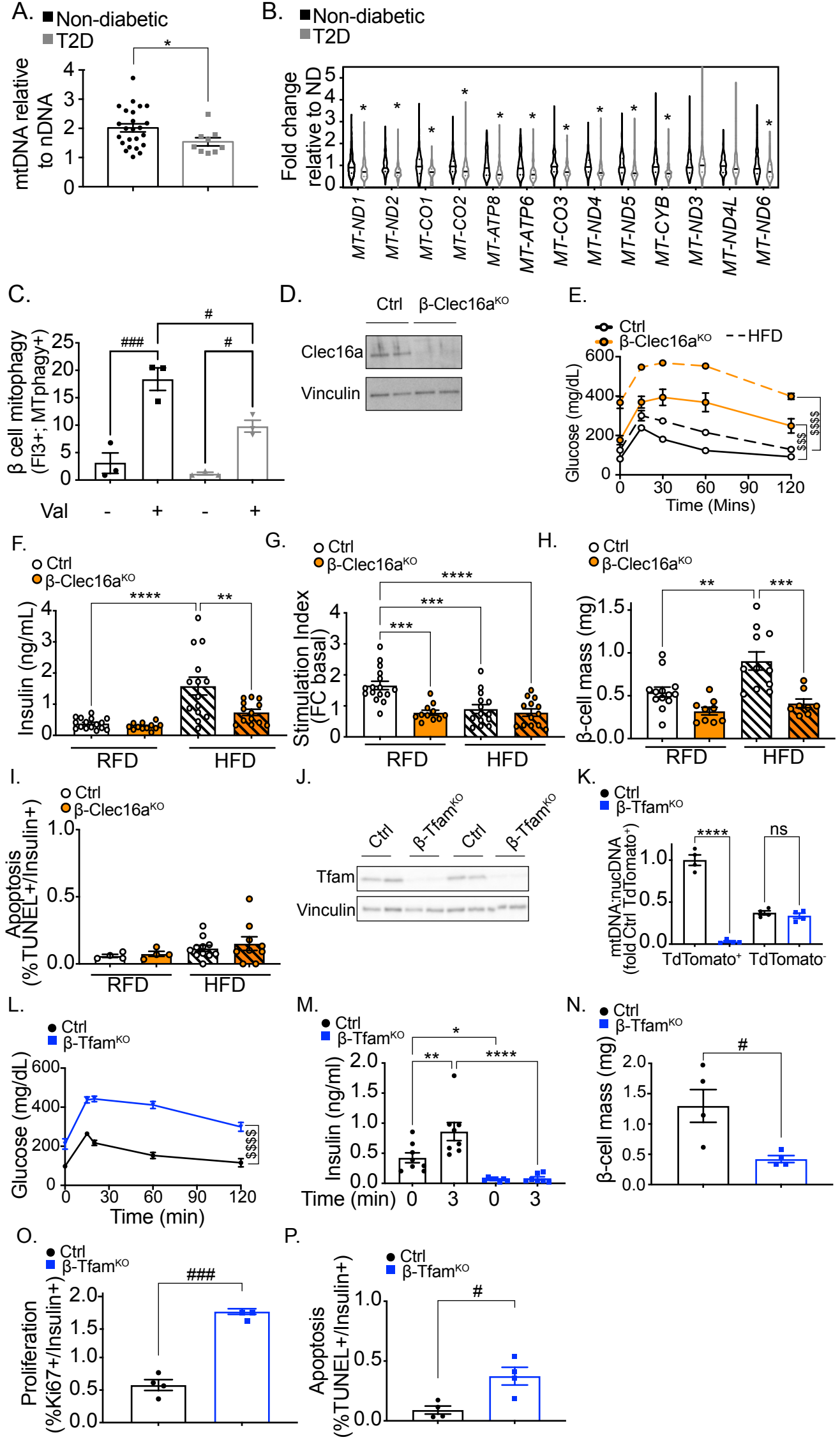

Figure 1: Mitochondrial quality control is impaired in β-cells in T2D and required for maintenance of glucose homeostasis and β-cell mass. (A) mtDNA:nuclear DNA ratio analysis of human islets from non-diabetic donors (n=24) or those with T2D (n=9). *p<0.05 unpaired Mann-Whitney test. (B) Violin plot showing levels of mitochondrially encoded RNA from single β-cell analysis[29] of human non-diabetic donors (ND) or those with T2D (n=3-5/group). *p<0.05 unpaired Mann-Whitney test. (C) Flow cytometry quantification of percentage of β-cells (Fluozin-3+) containing MTPhagy+ mitochondria from human islets of non-diabetic donors or those with T2D (n=3-4/group). p<0.05, ###p<0.001 one-way ANOVA Tukey's multiple comparison post-test. At least 2500 Fluozin-3+/DAPI- events quantified per sample. (D) Representative western blot (WB) demonstrating expression of Clec16a in islets isolated from 16-week-old Ctrl or Clec16a^{KO} mice. Vinculin serves as a loading control. n=4/group. (E) Blood glucose concentration measured during an IPGTT of Ctrl (black lines) or β-Clec16a^{KO} (orange lines) mice following 12-weeks regular fat diet (RFD; solid lines) or high fat diet (HFD; dashed lines). n=10-18mice per group, $$$p<0.001 Ctrl RFD vs β-Clec16a^{KO} RFD; $$$$p<0.0001 Ctrl HFD vs β-Clec16a^{KO} HFD by 2-way ANOVA. (F) Serum insulin levels following a 6hr fast. n=12-16 mice per group; **p<0.01, ****p<0.0001 one-way ANOVA, Tukey's multiple comparison post-test. (G) In vivo insulin secretion presented as stimulation index. n=12-16 mice per group; ***p<0.001 one-way ANOVA, Tukey's multiple comparison post-test. (H) Pancreatic β-cell mass from 12-week diet fed (16-week-old) Ctrl or β-Clec16a^{KO} mice. n=8-13 mice per group; **p<0.01 one-way ANOVA, Tukey's multiple comparison post-test. (I) β-cell apoptosis measured as the % of TUNEL+/Insulin+ cells. n=4-11 mice per group. (J) Representative WB demonstrating expression of Tfam in isolated islets from 10-week-old Ctrl or β-Tfam^{KO} mice. Vinculin serves as a loading control. n=4/group. (K) Quantification of mtDNA versus nuclear DNA from live FACS sorted islet cells of Ctrl (white bars) or β-TfamKO (blue bars) mice. n=4 mice per group; ****p<0.0001 one-way ANOVA, Tukey's multiple comparison post-test. (L) Blood glucose concentrations during an IPGTT of Ctrl (black lines) or β-Tfam^{KO} mice at 10-weeks of age. n=8-14 animals per group; $$$$p<0.0001 two-way ANOVA effect of genotype. (M) Serum insulin measured during in vivo glucose-stimulated insulin release in 10-week-old Ctrl (black circles) or β-Tfam^{KO} mice (blue squares). n=7-8 animals per group; *p<0.05, **p<0.05, ****p<0.0001 one-way ANOVA, Tukey's multiple comparison post-test. (N) Pancreatic β-cell mass from 12-week-old Ctrl (black circles) or β-Tfam^{KO} mice (blue squares). n=8-13 mice per group; #p<0.05 Student's unpaired t-test. (O) β-cell replication measured as the % of Ki67+/Insulin+ cells in 12-week-old mice. n=4 mice per group; ###p<0.001 Student's unpaired t-test. (P) β-cell apoptosis measured as the % of TUNEL+/Insulin+ cells. n=4-11 mice per group; #p<0.05 Student's unpaired t-test.

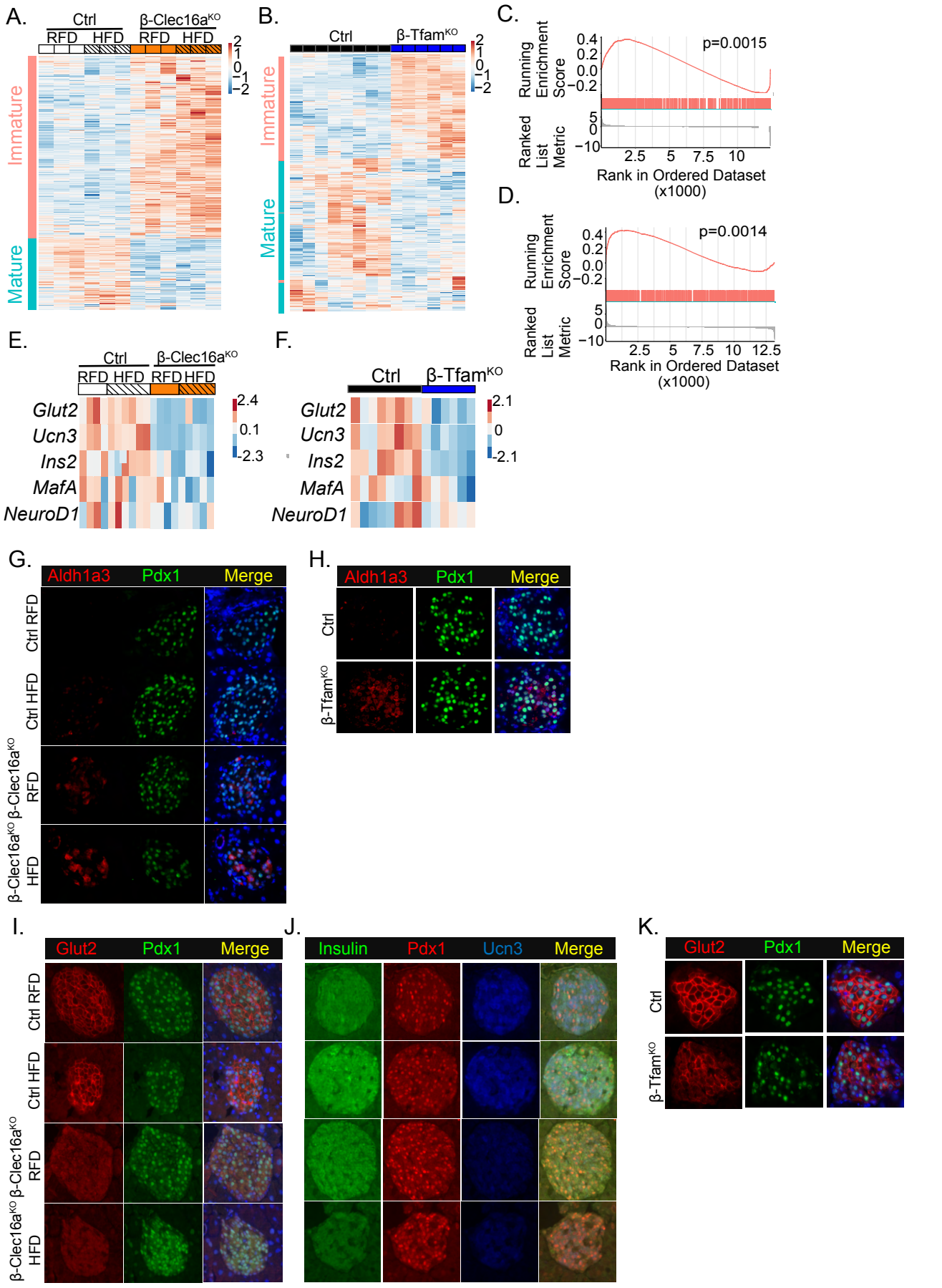

Figure 2. Mitochondrial dysfunction elicits β-cell immaturity. Expression heatmap of islet RNAseq from (A) Ctrl versus β-Clec16a^{KO} islets or (B) Ctrl versus β-Tfam^{KO} islets demonstrating expression of immature (pink) or mature (blue) gene markers (gene sets generated from [45]). Gene set enrichment analysis (GSEA; gene set generated from [45]) for expression of immature genes in β-Clec16a^{KO} versus Ctrl mice (C) or β-Tfam^{KO} versus Ctrl mice (D). (E) Heatmap displaying expression of core β-cell identity markers from Ctrl versus β-Clec16a^{KO} mice. (F) Heatmap displaying expression of core β-cell identity markers from Ctrl versus β-Tfam^{KO}. (G-I) Representative immunofluorescence images for key β-cell dedifferentiation markers in Ctrl and mitophagy-deficient or β-Tfam^{KO} islets. n=4-6/group. (G-H) Aldh1a3 (red), Pdx1 (green). (I-K) Representative immunofluorescence images for key β-cell maturity markers in Ctrl and mitophagy-deficient or β-Tfam^{KO} islets. n=4-6/group. (I) Glut2 (red), Pdx1 (green); (J) Insulin (green), Pdx1 (red), Ucn3 (blue); (K) Glut2 (red), Pdx1 (green).

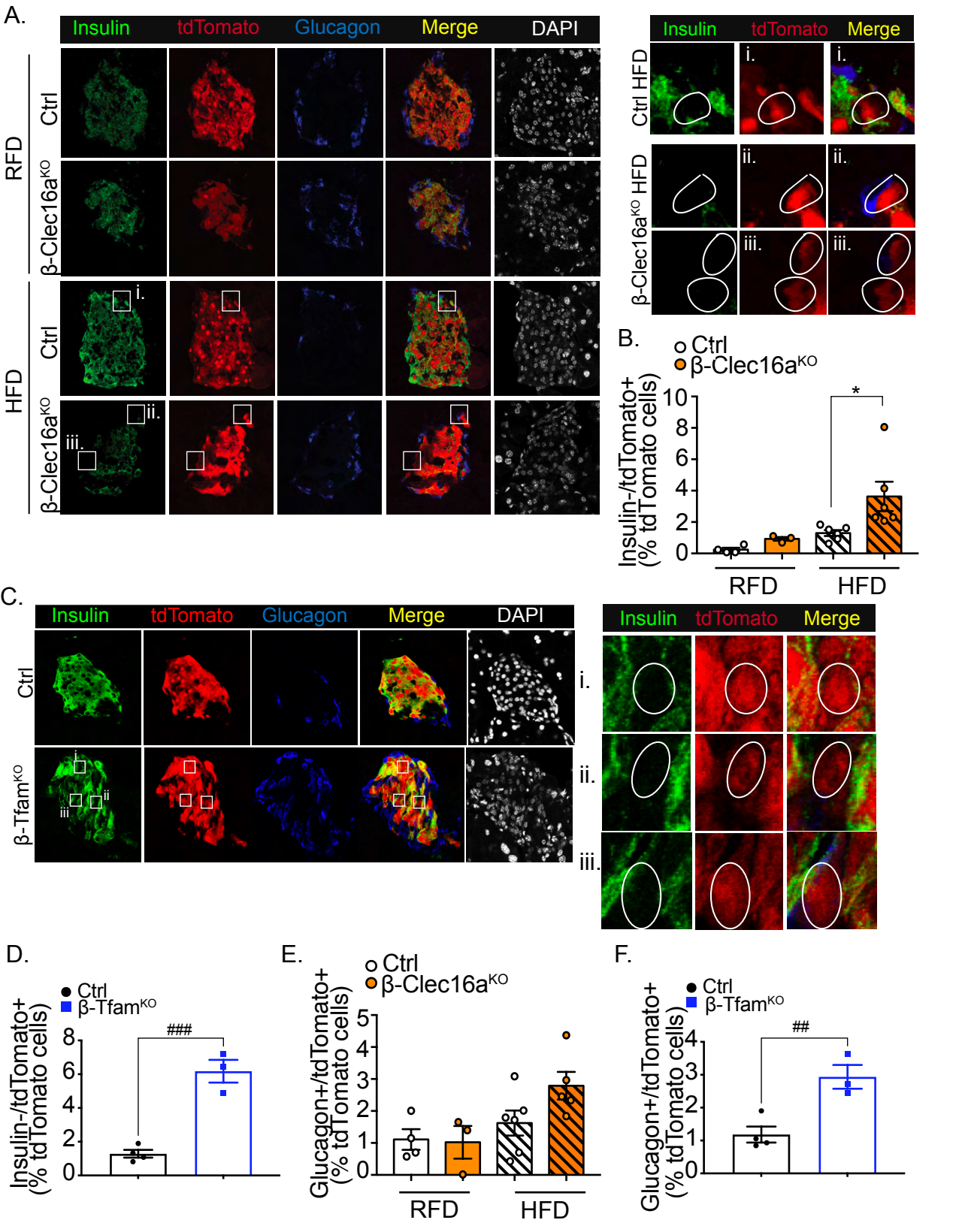

Figure 3. Lineage tracing studies implicate mitochondrial regulation of β-cell identity. (A-B) Lineage tracing results from *Ins1*-Cre;Rosa26-tdTomato and β-Clec16a^{KO};Rosa26-tdTomato mice. (A) Representative confocal immunofluorescence images showing staining with anti-Insulin (green), anti-Glucagon (blue) and endogenous tdTomato (red). Magnified images of white squares shown in i, ii, iii. (B) Quantification of Insulin-negative, tdTomato-positive cells. n=3-6 mice per group; *p<0.05 one-way ANOVA Tukey's multiple comparison post-test.(C-D) Lineage tracing results from *Ins1*-Cre;Rosa26-tdTomato and β-Tfam^{KO};Rosa26-tdTomato mice. (C) Representative confocal immunofluorescence images showing staining with anti-Insulin (green), anti-Glucagon (blue) and endogenous tdTomato (red). Magnified images of white squares shown in i, ii, iii. (D) Quantification of Insulin-negative tdTomato-positive cells. n=3-4 mice per group; ###p<0.001 Student's unpaired t-test. (E-F) Quantification of Glucagon-positive tdTomato-positive cells in *Ins1*-Cre;Rosa26-tdTomato and β-Clec16a^{KO};Rosa26-tdTomato mice (E) and β-Tfam^{KO};Rosa26-tdTomato mice (F). n=3-6 mice per group; ##p<0.01 Student's unpaired t-test.

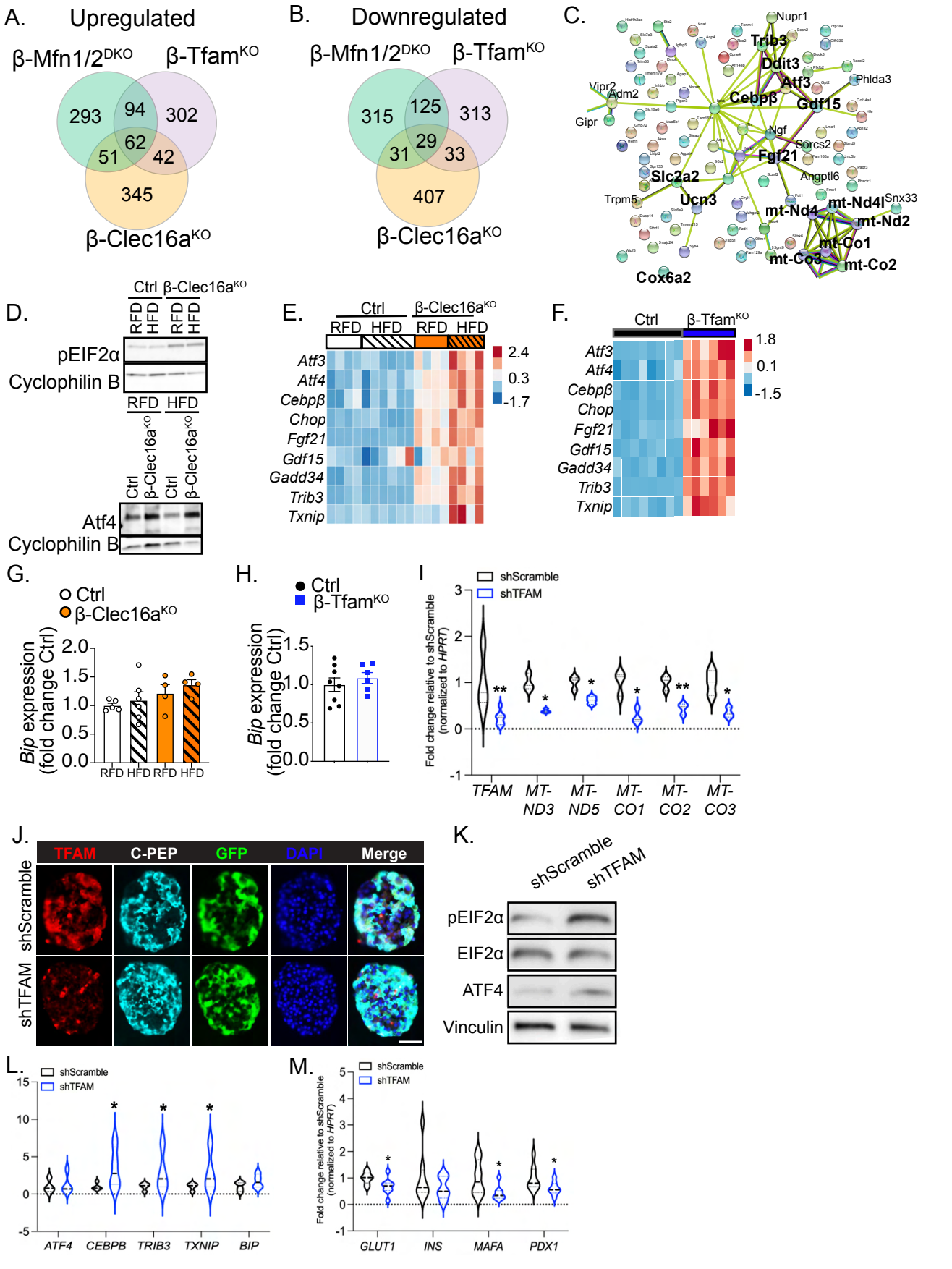

Figure 4. Mitochondrial dysfunction activates a shared transcriptional response in mouse and human islets. Comparative analysis of the top 500 upregulated (A) and the top 500 downregulated (B) genes across 3 models of β-cell-specific mitochondrial perturbations; mitophagy deficiency (β-Clec16a^{KO}), mtDNA depletion (β-Tfam^{KO}), and fusion deficiency (β-Mfn1/2^{DKO}). (C) STRING analysis of the 62 commonly upregulated and 29 commonly downregulated genes across all models. (D) Representative WB demonstrating expression of pEIF2α (top) and Atf4 (bottom) protein from Ctrl or β-Clec16a^{KO} islets fed RFD or HFD, cyclophilin B serves a loading control. n=3-4/group. (E) Heatmap generated from bulk RNA sequencing of Ctrl and β-Clec16a^{KO} islets after RFD or HFD displaying ISR gene expression. n=4-6 mice per group. (F) Heatmap generated from bulk RNA sequencing of Ctrl and β-Tfam^{KO} islets displaying ISR gene expression. n=6-8 mice per group. (G) *Bip* expression from bulk RNA sequencing of Ctrl or β-Clec16a^{KO} islets after RFD and HFD. n=4-6 mice per group. (H) *Bip* expression from bulk RNA sequencing of Ctrl and β-Tfam^{KO} islets. n=6-8 mice per group. (I) qPCR analysis of TFAM and mtRNAs in shScramble or shTFAM-expressing human pseudoislets. n=8/group; *p<0.05, **p<0.001 Student's unpaired t-test. (J) TFAM protein expression by immunostaining in shTFAM compared with shScramble human pseudoislets. C-peptide marks β cells. Scale bar=50micrometers, n=4/group. (K) Expression of pEIF2α, total EIF2α and ATF4 protein by WB from shScramble or shTFAM human pseudoislets. Vinculin serves a loading control. n=3/group. (L) ISR target genes, *BIP* expression and (M) β cell markers by qRT-PCR in shScramble or shTFAM human pseudoislets. n=4-8/group; *p<0.05 Student's unpaired t-test.

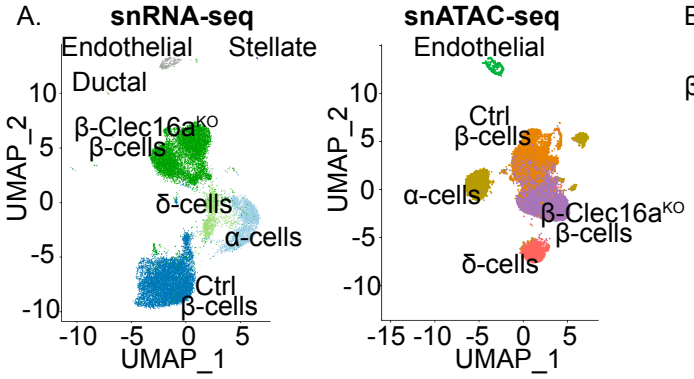

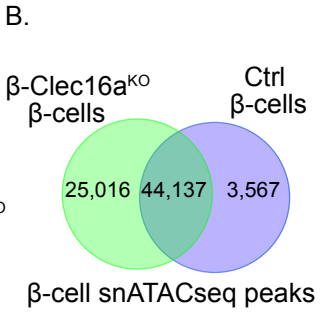

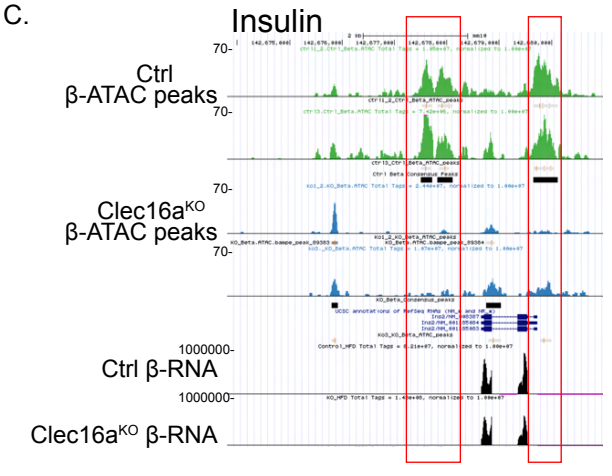

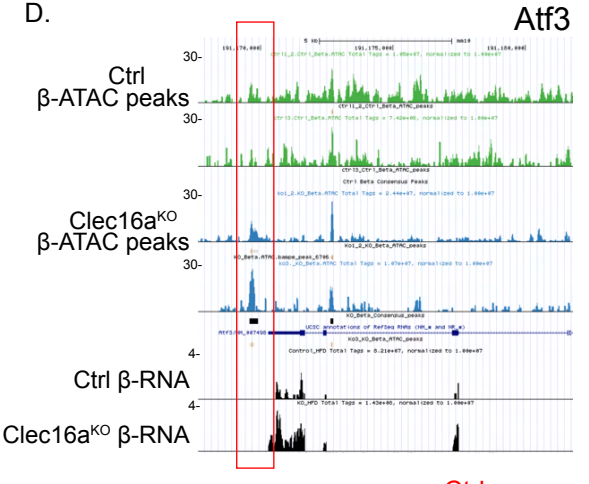

E.

TFs enriched in Ctrl β-cell ATAC peaks

Rank	Motif	Name
1		CTCF(Zf)
2		BORIS(Zf)
3		NeuroD1(bHLH)
4		Atoh1(bHLH)
5		Olig2(bHLH)
6		Ptf1a(HLH)
7		Sp1(Zf)

TFs enriched in β-Clec16a^KO β-cell ATAC peaks

Rank	Motif	Name
1		Chop(bZIP)
2		Atf4(bZIP)
3		BATF(bZIP)
4		Atf3(bZIP)
5		Jun-AP1(bZIP)
6		AP-1(bZIP)
7		CEBP-AP1(bZIP)
8		Bach2(bZIP)

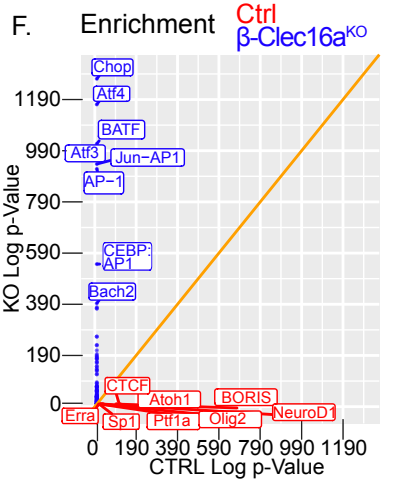

Figure 5. Loss of mitochondrial quality control induces chromatin remodeling. (A) UMAP plots of snRNA-seq from Ctrl and β-Clec16a^{KO} islet cell nuclei (left) and snATAC-seq (right) from Ctrl and β-Clec16a^{KO} islet cell nuclei. n=4. (B) Venn diagram of common and unique open chromatin regions from snATAC-seq of Ctrl and β-Clec16a^{KO} β-cell nuclei. (C) Representative *Ins2* snATAC- and β-cell pseudobulk snRNA expression-peaks from Ctrl (1st and 3rd tracks) and β-Clec16a^{KO} (2nd and 4th tracks). (D) Representative *Atf3* snATAC- and β-cell pseudobulk snRNA expression-peaks from Ctrl (1st and 3rd tracks) and β-Clec16a^{KO} (2nd and 4th tracks). (E) HOMER analysis of Ctrl β-Cell ATAC peaks showing enrichment of motifs corresponding to zinc finger (Zf) and beta-Helix Loop Helix (bHLH) identity factors (left) and β-Clec16a^{KO} β-Cell ATAC peaks showing enrichment of motifs corresponding to bZIP stress response factors (right). n=4. (F) Visualization of the top 8 enriched TF motifs from Ctrl β-cell specific ATAC peaks (red) and β-Clec16a^{KO} β-cell specific ATAC peaks (blue). n=4.

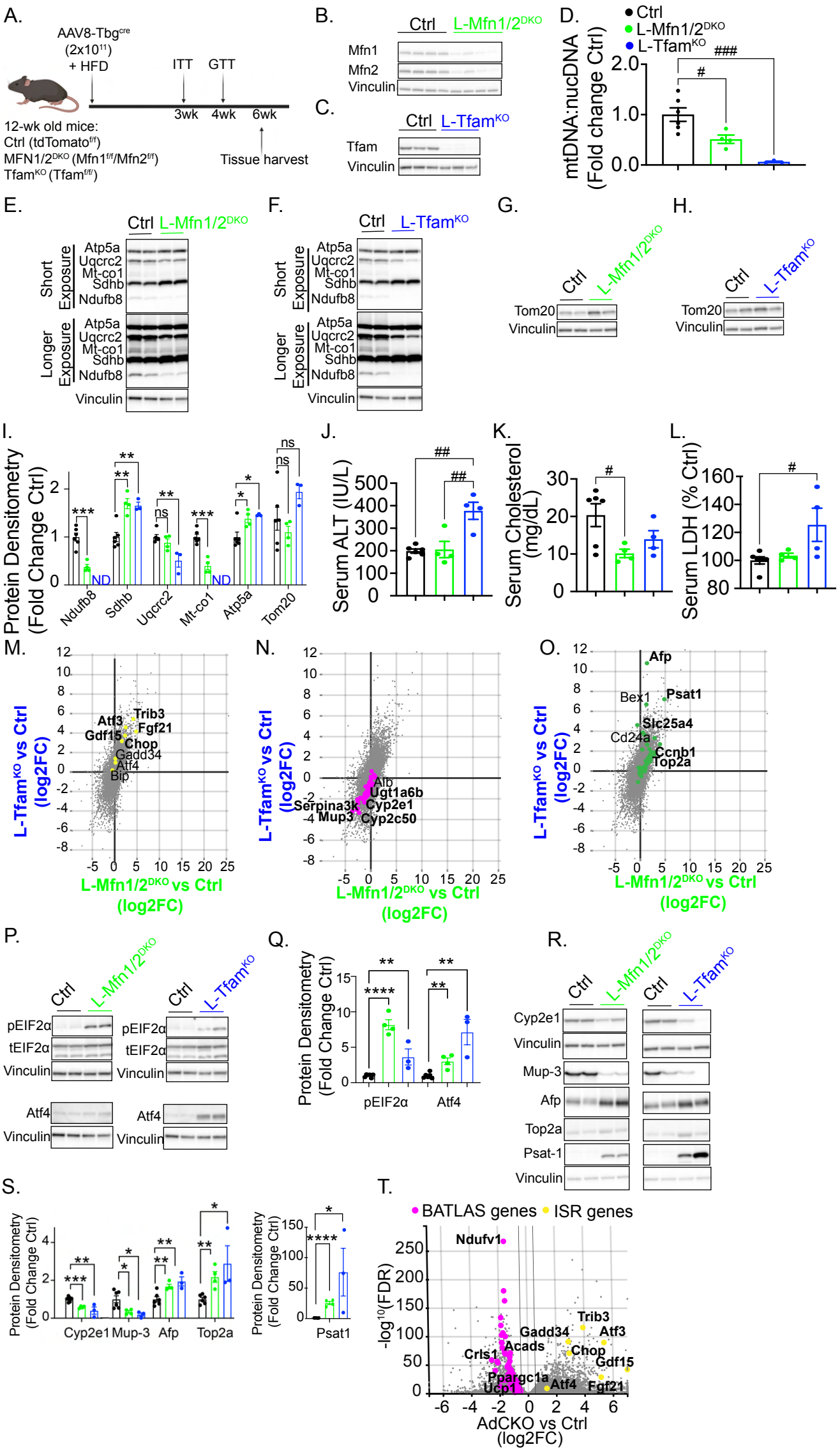

Figure 6. Mitochondrial dysfunction commonly induces the ISR and immaturity across several metabolic tissues. (A) Schematic diagram illustrating the experimental design of AAV8-Tbgcre delivery and analysis of liver-specific loss of mitochondrial fusion (L-Mfn1/2^{DKO}) and mtDNA copy number control (L-Tfam^{KO}). (B) Protein expression of Mfn1 and Mfn2 by WB in liver from Ctrl (AAV8-Tbg^{cre}) and L-Mfn1/2^{DKO} mice. (C) Protein expression of Tfam by WB in liver from Ctrl (AAV8-Tbg^{cre}) and L-Tfam^{KO} mice. (D) Quantification of mtDNA to nuclear DNA ratio in liver by qPCR. n=4-6 animals per group; #p<0.05 one-way ANOVA Tukey's multiple comparison post-test. Protein expression of murine OXPHOS complex subunits in liver from (E) Ctrl and L-Mfn1/2^{DKO} and (F) Ctrl and L-Tfam^{KO} mice by WB. Vinculin serves as a loading control. Protein expression of Tom20 in liver from (G) Ctrl and L-Mfn1/2^{DKO} and (H) Ctrl and L-Tfam^{KO} mice by WB. Vinculin serves as a loading control. (I) Densitometry quantification of OXPHOS subunits and Tom20 from (E-I). n=3-6 mice per group; *p<0.05, **p<0.01, ***p<0.001 student's unpaired t-test vs Ctrl. ND=not detected. (J-L) Serum liver function analyses from AAV8-Tbg^{cre} Ctrl (black bars), L-Mfn1/2^{DKO} (green bars) and L-Tfam^{KO}. (J) Serum ALT; ##p<0.01 one-way ANOVA Tukey's multiple comparison post-test. (K) Circulating serum cholesterol levels; #p<0.05 one-way ANOVA Tukey's multiple comparison post-test. (L) Circulating serum LDH levels; #p<0.05 one-way ANOVA Tukey's multiple comparison post-test. (M-O) Differential gene expression comparison plots of Ctrl vs either L-Tfam^{KO} (y-axis) or L-Mfn1/2^{DKO} (x-axis) showing similarly upregulated ISR genes (M), immaturity genes[73] (N), and similarly downregulated maturity genes[73] (O). Select gene expression changes reaching statistical significance in both L-Mfn1/2^{DKO} and L-Tfam^{KO} mice are noted in bold font. (P) Protein expression of pEIF2α (top panels) or Atf4 (bottom panels) in Ctrl, L-Mfn1/2^{DKO} and L-Tfam^{KO} liver. Vinculin and tEIF2α serve as loading controls. (Q) Densitometry of pEIF2α and Atf4 protein levels. n=3-6 mice per group; **p<0.01, ****p<0.0001 Student's unpaired t-test vs Ctrl. (R) Protein expression of mature (Mup-3, Cyp2e1) and immature (Top2a, AFP and Psat-1) hepatocyte markers from liver of Ctrl, L-Mfn1/2^{DKO} and L-Tfam^{KO} mice. Vinculin serves as a loading control. (S) Densitometry of immature and mature protein levels shown in (R). n=3-6 mice per group; *p<0.05, **p<0.01, ***p<0.001, ****p<0.0001 Student's unpaired t-test vs Ctrl. (T) Volcano plot of differential gene expression in Ctrl vs AdCKO (adiponectin Cre-driven Crls1 knock-out) brown fat showing upregulated ISR genes (yellow circles) and downregulated BATLAS brown fat maturity genes (pink circles; generated from [77]).

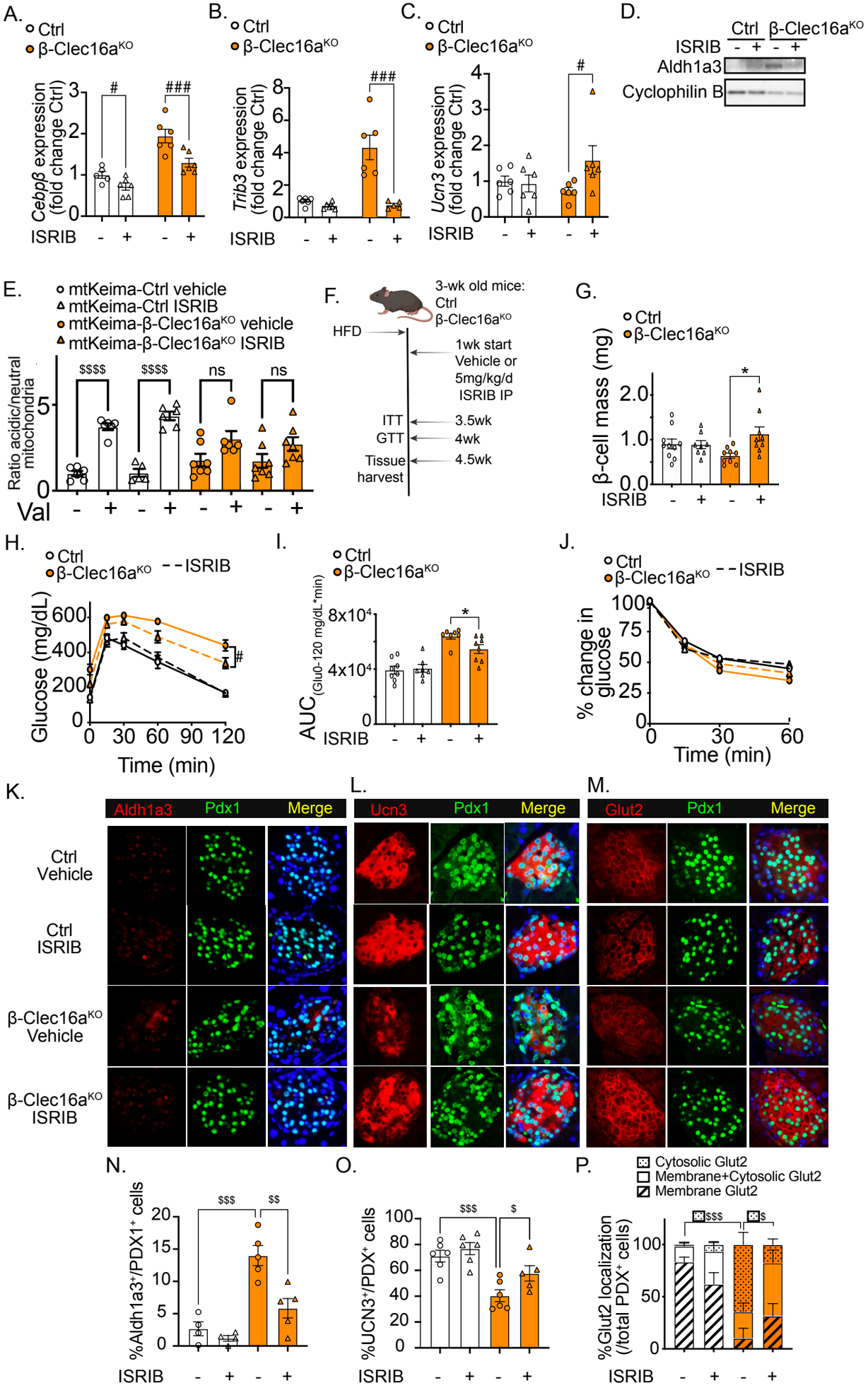

Figure 7. Pharmacologic blockade of mitochondrial retrograde signaling in vivo restores β-cell mass and maturity. (A-C) qPCR of Ctrl (white bars) or β-Clec16a^{KO} (orange bars) islets treated ex vivo with (triangles) or without (circles) ISRIB. n=6/mice per group; #p<0.05, ###p<0.01 2-way ANOVA Sidak's multiple comparison posttest effect of drug within genotype for ISR targets *Cebpβ* and *Trib3* (A-B) and β-cell maturity marker *Ucn3* (C). (D) Protein expression of Aldh1a3 by WB from Ctrl or β-Clec16a^{KO} islets treated ex vivo with ISRIB, Cyclophilin B was used as a loading control. (E) Ratio of acidic to neutral compartment localized mitochondria from β-cells from mtKeima-Ctrl (white bars) or mtKeima-β-Clec16a^{KO} (orange bars) mice treated with (triangles) or without (circles) ISRIB ex vivo for 24hr. n=5-7mice per group; $$$$p<0.0001 one-way ANOVA Tukey's multiple comparison post-test. (F) Schematic diagram illustrating the experimental design of in vivo ISRIB treatment and analysis of Ctrl or β-Clec16a^{KO} mice. (G-J) Results from Ctrl (white) or β-Clec16a^{KO} mice (orange) treated with ISRIB (triangles) or Vehicle (circles) once daily for 4-weeks. n=8-10 mice per group; #p<0.05 2-way ANOVA effect of ISRIB within genotype. *p<0.05 Student's unpaired t-test. (G) Pancreatic β-cell mass. (H) Blood glucose concentrations during an IPGTT. (I) AUC calculated from IPGTT data. (J) Blood glucose levels during an ITT. (K-M) Representative pancreatic immunofluorescence images from Ctrl or β-Clec16a^{KO} mice treated in vivo with Vehicle or ISRIB. (K) Sections stained with antibodies against Aldh1a3 (red), Pdx1 (green), and DAPI (blue). (L) Sections stained with antibodies against Ucn3 (red), Pdx1 (green), and DAPI (blue). (M) Sections stained with antibodies against Glut2 (red) Pdx1 (green), and DAPI (blue). (N-P) Quantification of staining for (N) % cytosolic Aldh1a3+ / Pdx1+ cells. n=4-5 mice per group; $$p<0.01 one-way ANOVA Tukey's multiple comparison post-test; (O) %Ucn3+/Pdx1+ cells. n=5-6 mice/group; $p<0.05, $$$p<0.01 one-way ANOVA Tukey's multiple comparison post-test; and (P) Glut2 localization, classified as all cytosolic (Cytosolic), mixed cytosolic and plasma membrane (Membrane+Cytosolic) and all plasma membrane (Membrane) as a % of all Pdx1+ cells. n=6 mice/group; $p<0.05, $$$p<0.01 one-way ANOVA Tukey's multiple comparison post-test (cytosolic localized Glut2).